2017-01-01

Design And Development Of A High Pressure Oxy-Methane Combustor

Jaime Cruz Gurrola
University of Texas at El Paso, jaimecg92@gmail.com

DESIGN AND DEVELOPMENT OF A HIGH PRESSURE OXY-METHANE COMBUSTOR

JAIME CRUZ GURROLA

Master's Program in Mechanical Engineering

APPROVED:

Norman D. Love, Ph.D., Chair

Ahsan Choudhuri, Ph.D.

Luis R. Contreras, Ph. D.

Charles Ambler, Ph.D.
Dean of the Graduate School

Dedication

To my parents, Jaime and Betty, to my sister Diana, to my brother Kike, and to my girlfriend Lily. For always giving me their support and being there for me. Without you nothing of this would’ve been possible.

DESIGN AND DEVELOPMENT OF A HIGH PRESSURE OXY-METHANE COMBUSTOR

by

JAIME CRUZ GURROLA, BSME

THESIS

Presented to the Faculty of the Graduate School of

The University of Texas at El Paso

in Partial Fulfillment

of the Requirements

for the Degree of

MASTER OF SCIENCE

Department of Mechanical Engineering

THE UNIVERSITY OF TEXAS AT EL PASO

August 2017

Acknowledgements

I would like to thank my advisor Dr. Norman Love for giving me the opportunity to work and do research in the cSETR. It was a challenging and rewarding work where I learned more than ever before. He was always helpful and I appreciate his guidance and mentorship throughout my graduate studies.

Special recognition also goes to my team members and people who have worked with me including Arifur Chowdhury, Jad Aboud, Ana Rios, Mohieminul Khan, Joel Quintana, Luz Bugarin, Armando Ochoa, Bryan Morales, Mehrin Chowdhury, Luisa Cabrera, Brian Lovich, George Quinones, Ana Luisa Garcia, and friends in the casita and water break. You guys made this a great experience.

I'd also like to thank Mr. Hill for always giving us a rough time. He was harsh when necessary but I learned a lot from him regarding project management and engineering.

Thanks to my roommates with whom I've lived together since the beginning of my undergraduate studies. You are like brothers to me and have made living far away from home much easier.

Finally, I'd like to thank Air Liquide for funding this project and Hwanho Kim for giving us his technical guidance.

Abstract

Most of the greenhouse gas emissions in the US comes from the electricity sector by burning fossil fuels. Environmental regulations have been implemented to reduce the amount of CO_2 emitted into the atmosphere. One method to reduce the greenhouse gas emissions to the atmosphere is oxy-fuel technology. One of the biggest challenges of oxy-fuel combustion is thermal management due to the elevated temperature combustion. The main objective of this thesis was to design and develop a steady-state high pressure combustor that uses oxygen and methane with a thermal power input of 500 kW and operation at 20 bar pressure. An existing high-pressure combustor at UTEP was modified to meet the requirements by using both analytical and numerical analysis (FEA and CFD). To withstand the combustion temperatures, it was proposed that a high velocity ring of CO_2 be injected along the inner walls of the combustion chamber. It was found through the CFD analysis that the injection of CO_2 would effectively shield and maintain an allowable temperature at the inner walls of the combustor only for ¾ of the total length of the combustion chamber. To cool down the injector face and the end plates, an active water cooling solution was proposed.

Table of Contents

List of Tables

List of Figures

Chapter 1: Introduction and Background

1.1 – Introduction

According to the United States Environmental Protection Agency (EPA), in 2015 there were 6587 million metric tons of CO_2 equivalent greenhouse gas emissions into the atmosphere. Greenhouse gases are harmful because they trap the heat in the atmosphere and lead to higher temperatures on the planet. Greenhouse gases include carbon dioxide, methane, nitrous oxide, and fluorinated gases and they come from various sources such as electricity generation, transportation, industry, commercial and residential, and agriculture. As seen in Figure 1.1, the biggest source of greenhouse gas emissions in the US came from electricity generation, accounting for 29% of the total emissions [1].

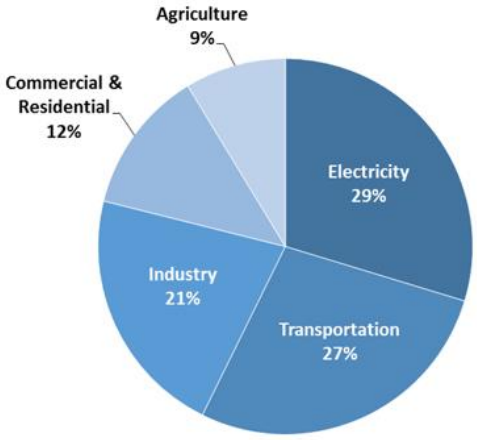

Figure 1.1 - Total U.S. Greenhouse Gas Emissions by Economic Sector in 2015[1].

Due to their abundance and low cost, approximately 65% of the electricity in the US is generated by burning fossil fuels such as coal, natural gas, and petroleum which leads to the high amounts of greenhouse gases created by the electricity generation sector. The rest of the electricity comes from nuclear power and renewable sources, accounting for 20% and 15%, respectively. From the total use of fossil fuels, 34% come from natural gas, 30% from coal, and 1% from petroleum. It is important to point out that due to recent discovery of natural gas resources, its low

price, and lower emissions, the use of natural gas increased from 26% to 34% from 2015 to 2016, replacing coal as the largest amount of fossil fuel consumed to generate electricity in the U.S.[2][3].

Natural gas, which consists mostly of methane (CH_4), can be used to generate electricity using three main different methods which are: steam generation power plants, simple cycle plants, and combined cycle plants. In a steam generation power plant, natural gas is burned in a boiler to heat water which produces steam that then turns a turbine to generate electricity. In a simple cycle plant, natural gas is burned and the high temperature exhaust gases are pressurized and sent to a gas turbine to generate electricity. Simple cycle plants have a fast start up time so they are generally used at peak load times where more electricity is demanded. However, simple cycle plants are less efficient than steam power plants. Combined cycle plants are similar to simple cycle plants. However, the heat that would normally be released to the ambient, is recovered and used to heat water and run a steam turbine. These types of plants generally have efficiencies higher than 50% [4].

Recently, there has been a big growth in the renewable energy sector, solar energy has especially gained attention and has grown significantly due to price reduction to produce photovoltaic cells. However, solar energy and renewable resources are still far from being the major source for electricity both globally and in the U.S. A forecast from the U.S. Energy Information Administration (EIA) predicts a 48% increase for solar from 21 GW at the end of 2016 to 32 GW at the end of 2018, accounting for only about 1% of the total electricity production[5]. Another projection made by the EIA estimates that the use of natural gas for the electric power sector will increase 2.2% per year from 2010 to 2040[6]. The reason for this significant increase is because natural gas is an appealing option for new power plants due to its fuel efficiency. Natural gas also has lower emissions than coal or petroleum and as governments start implementing tighter regulations to reduce CO_2 emissions, they may favor the use of natural gas instead of other fossil fuels [6].

It is clear that for the near term future, the US and the world will still rely primarily on using fossil fuels to generate electricity. Therefore, there is in an immediate need to lower the greenhouse gas emissions from fossil fuels. The Intergovernmental Panel on Climate Change (IPCC) proposed several areas in order to reduce greenhouse gas emissions coming from the electricity sector which include: a) increased efficiency of power plants and fuel switching, b) renewable energy, c) increased energy efficiency transmission, d) nuclear energy, and e) carbon capture sequestration and storage (CCS)[7]. To increase the efficiency of power plants, conventional coal powered steam turbines may need to be converted to an advanced turbine based system that uses pulverized coal. Another option may to use natural gas as a fuel, which is lower in cost and typically produces less emissions. The third option may be to convert simple cycle plants into combined cycle plants. Carbon capture and sequestration is a strategy that is also currently being investigated to reduce GHGs from fossil fuels into the atmosphere. This technology will be discussed more in Section 1.3.

1.2 – NATURAL GAS VS. COAL

It has been established that fossil fuels will continue to be used for an extended period of time. Therefore, it is important to understand the advantages and disadvantages of using natural gas or coal for power generation. In general, natural gas is a fuel that burns cleaner than coal. Natural gas has lower emissions of CO_2 and nitrogen oxides (NOx) compared to coal. However, coal's emissions also have sulfur dioxide (SO_2) and significant amounts of particulate matter, both of which are also harmful to the environment. In 2015, coal accounted for 34% of the electricity generated in the US and 70% of the total CO_2 emissions to the atmosphere [1].

A study of cost and performance for fossil energy plants by the National Energy Technology Laboratory (NETL) in 2015 shows that natural gas plants are more efficient than coal plants[8]. As seen in Figure 1.2, natural gas combined cycle (NGCC) plants have the highest efficiency even when taking into account CO_2 capture. A NGCC plant with carbon capture is still more efficient with an efficiency of 45.7%. For comparison purposes, supercritical pulverized coal

(SCPC) with no carbon capture produces a 40.7% efficiency. Carbon capture brings more costs to power plants, implementation further reduces the efficiency. NGCC power plants lose 6% whereas SCPC lose 8% when carbon capture is implemented in the system.

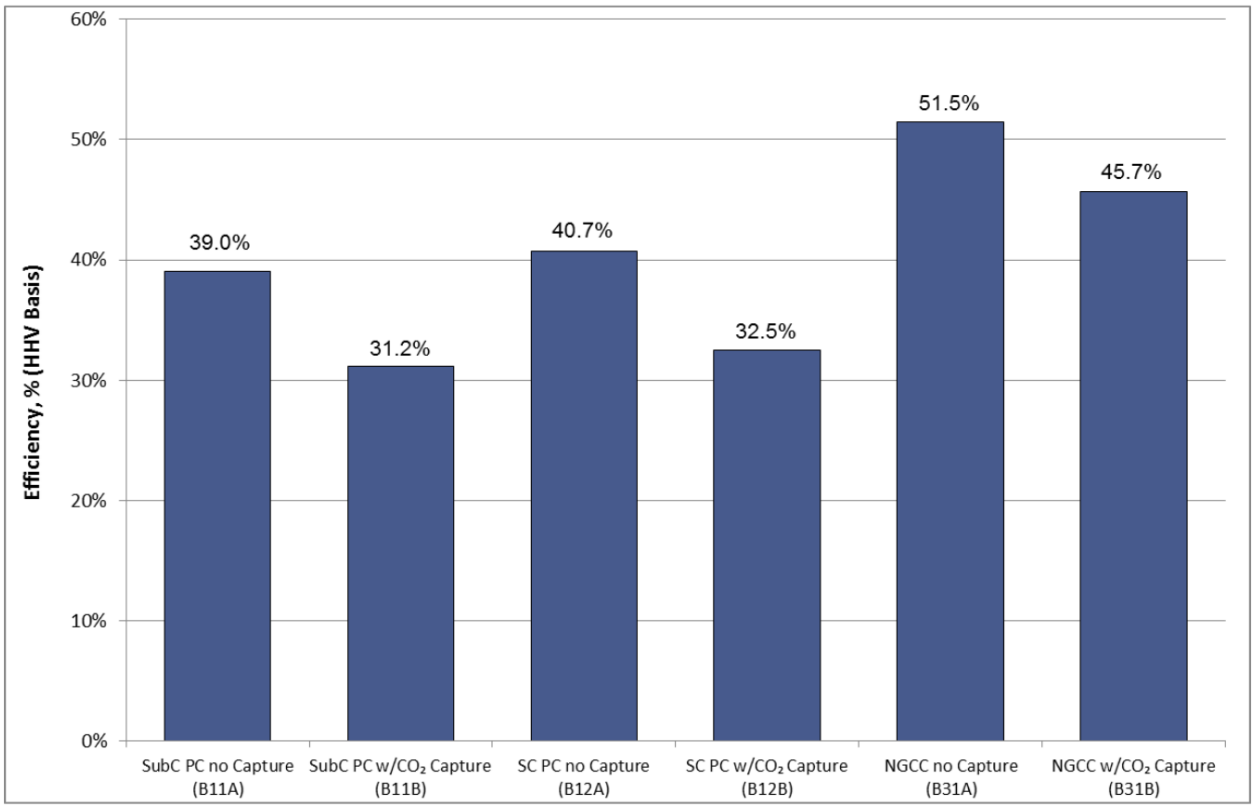

Figure 1.2 - Efficiency of different configurations of power plants[8].

The same study also reveals that raw water usage in NGCC plant is lower than in a SCPC plant. Therefore, it can be concluded that the NGCC plant may be better overall for the environment due to higher efficiencies, lower environmental emissions, and less water use. For these reasons, the use of natural gas for electricity production is a topic that should be investigated due to the many benefits associated with the use.

1.3 – Carbon Capture Sequestration and Storage

CCS is a method to reduce the GHG emissions to the atmosphere. After the CO_2 has been captured, it is compressed and transported to a storage site. Then the CO_2 is typically injected

underground where high pressures keep the CO_2 compressed over time. These sites are usually natural geological formations or empty location of harvested fossil fuels [9].

The three main ways to capture CO_2 include i) pre-combustion, ii) post-combustion, and iii) oxy-fuel combustion.

Pre-combustion capture is a process where the fuel is turned into a synthesis gas containing mostly carbon monoxide (CO) and hydrogen. Different types of processes are used to create the synthesis gas depending if the fuel source is solid, liquid, or gas. The CO is then converted into CO_2 through a reaction that also produces hydrogen. The hydrogen can then also be used as a fuel in the plant. Afterwards, the CO_2 can be separated and compressed or liquefied for easier transportation[9].

Post-combustion is the process of capturing CO_2 after combustion has happened. After the flue gas from combustion is desulphurised, it is sent to a scrubbing agent. This scrubber absorbs the CO_2 from the flue gas and is later separated from the scrubbing agent and can be stored to be transported underground. The benefit of this method is that it can be easily retrofitted to existing power plants and help reduce CO_2 emissions. However, the disadvantages are the low concentration of CO_2 in the flue gas (20% or less) and the electricity cost to compress the CO_2 for storage because combustion happens at atmospheric pressure[10][11].

1.4 – Oxy-Fuel Combustion

Conventional combustion involves a fuel and an oxidizer, where air is typically utilized as the oxidizer. Air is primarily a mixture of 77% nitrogen and 23% oxygen. Oxy-fuel combustion differs from conventional combustion in that the oxidizer used is oxygen in concentrations from 95-99%. By using oxygen as an oxidizer, several benefits can be gained. One advantage of oxy-fuel combustion is that in many cases, it may be retro fit into existing power plants.

In addition, when using oxygen, nitrogen is eliminated from the oxidizer stream. Eliminating nitrogen means that NOx emissions in the flue gas are greatly reduced, which is a source of acid rain and smog[12]. Assuming a complete combustion, and use a fuel with reduced

nitrogen content, such as natural gas, the primary products are water vapor and carbon dioxide. Another benefit of eliminating nitrogen is a large reduction in volume of the flue gases. By removing nitrogen, the volume of the flue gas in oxy-fuel combustion is about 75% less than the volume of air-fuel combustion[13]. Flowing a lower volume of gas translates into reduced equipment size and may result in less initial and operating costs. Another benefit includes making CO_2 purification more efficient, since flue gases are typically< 99%.

However, there are also challenges that need to be overcome regarding oxy-fuel combustion. Combusting CH_4 with air yields a temperature of around 2200 K, but oxy-combustion yields adiabatic flame temperatures near 3500 K. A higher temperature theoretically means that higher efficiencies may be achieved, but the materials used in the construction of the equipment currently are not able to withstand these elevated temperatures for extended periods of time. Therefore, flue gases are typically recirculated and mixed with the inlet gases to regulate the temperature of the flame. By recirculating the flue gases, higher concentrations of CO_2 are recovered in the flue gases, reducing some of the parasitic efficiency load on the system[14].

The cost of electricity to create O_2 is another challenge for oxy-combustion systems. To create oxygen, an air separation unit (ASU) is needed. The ASU separates the oxygen from the air using cryogenic temperatures, but the cost of electricity to do this is high and may reduce the economic advantage of efficiency gains possible in an oxy-combustion system. Studies have shown that the ASU process in oxy-combustion plants consume 25-30% of the power outputs, thus increasing the cost of electricity by 40-50%[15]. Praxair is investigating another way to produce oxygen at a much lower cost using an oxygen transport membrane[14]. For this reason, to make oxy-fuel a viable option, the cost of producing oxygen must be reduced or the efficiency has to be increased[16]. However, the efficiency and viability of an oxy-fuel can vary on other factors such as current fuel prices and location[16].

Thus, three main benefits are associated with high pressure oxy-fuel combustion: a) increased efficiency because the latent heat in the flue gas can be recovered, b) equipment size and

cost may be reduced from oxy-combustion due to high pressure and gas volume reduction, and c) no air in-leakage increases CO_2 purity thus reducing CO_2 purification costs[13].

1.5 – OBJECTIVE

The main objective of this thesis is to design a high-pressure combustor (HPC) capable of continuous operation up to 500 kW firing input and up to 20 bar chamber pressure utilizing oxy-methane combustion. To meet the project's objective, an existing combustor at The University of Texas at El Paso's (UTEP) Center for Space Exploration Technology Research (cSETR) laboratory will have to be modified. The following tasks will be carried out:

1. Design of injectors/burners with additive manufacturing.
2. Provide a structural analysis of the combustor.
3. Provide a thermal analysis of the combustor.
    a. Develop a cooling system for the inner walls of the combustor.
    b. Develop a cooling system for the injection face.
    c. Develop a cooling system for the exit plates.
4. Redesign of inlet and exit caps, instrumentation ports, and windows.

1.6 – PRACTICAL RELEVANCE

The high-pressure combustor will help to better understand the combustion stability and emissions of varying oxy-fuel gas mixtures at elevated pressure and temperature. Due to the high temperature associated with oxy-fuel combustion, this type of combustor could be used in boilers, where the high temperature generated can be utilized to convert the water into steam instead of being sent to the atmosphere as waste. The HPC will also be able to be utilized to gather flame imaging. Chamber pressure will be able to me manipulated using a modular/removable exit nozzle. The HPC will also have the capability of testing different mixture ratios through its control system. Understanding flame characteristics, emissions, and cooling system requirements of oxy-fuel

combustion at high pressure and temperature is important for the advancement of cleaner technologies and the development of future combustors.

Chapter 2: Literature Review

To design the combustor, it is important to know the research and designs that have been developed in the past. This chapter will focus on the design and operating conditions of existing high-pressure combustors and oxy-fuel combustors. Similarities and differences between existing combustors and this design will be discussed. A better understanding and background of existing injector designs, cooling systems, pressure control, and feed systems are the goals of this literature review. The existing high-pressure combustor at UTEP will also be discussed in detail.

2.1 – Existing Combustor Designs

Slabaugh et. al have developed an optically accessible combustor capable of up to 3 MW thermal power and up to 40 bar chamber pressure. This experiment is used to gather optical measurements at realistic gas turbine conditions. The oxidizer used was air, however there is no specification of what fuel was used. To keep the combustor cooled, a regenerative water cooling system is used. All the inner surfaces of the combustion chamber are covered with a thermal barrier coating to reduce the temperature of the steel. Finally, a preheated nitrogen film is flown over the window to protect it from the heat. Instrumentation and control requirements are mentioned but there is no diagram of the feed system. To control the pressure inside the chamber, an electronically actuated butterfly valve is used. This valve is kept under 600 K by injecting transverse jets of high pressure water into the main flow. The combustor design was validated through experimentation and is capable of optical measurements of flow velocity, species concentrations, and flow temperature[17].

NETL has a high-pressure combustion facility with two test rigs. The first one is the dynamic gas turbine test rig and it is used to simulate gas turbine conditions with acoustic feedback. This test rig can operate at 10 atm pressure using natural gas and liquid fuel. The second test rig is called the SimVal and is used for simulation validation. It is an optically accessible combustor capable of 22 atm pressure using natural gas and hydrogen as fuels, with an inlet temperature of up to 700 K. Using these test rigs, NETL is capable of emissions analysis of NOx,

CO, CO_2, O_2, and allows for use of a mass spectrometer. NETL is also able to gather data of flame structure and flow field characterization[18]. However, no detailed information is presented on the design of the test rigs.

Gomez et. al have developed the first phase of an optically accessible test rig to simulate gas turbine conditions. The final design is proposed to operate with an inlet temperature of 650 K, pressures up to 9.28 bar, and air inlet flows of 1.27 kg/s. The presented design is the first phase and will only be able to operate at atmospheric conditions. The objective is to generate data that can be used to validate computational models and improve combustor thermal management. The combustor has an inner diameter of 8 inches and uses air as the oxidizer. The test rig uses lean premixed fuel and uses a swirl nozzle to mix the gases, but there is no specification of the fuel used. Back pressure valves are used to control the pressure in the system. To keep the temperature within material limits, air is pushed between two concentric quartz cylinders and into a metal cooling jacket afterwards. Metal sections of the combustion chamber are also covered with a zirconia thermal barrier coating. The paper also provides a schematic of the feed system and selected instrumentation[19].

De Persis et. al have studied the effects of O_2 enrichment and CO_2 dilution on laminar methane flames. The tests were done at 300 K and atmospheric conditions using air with different concentrations of O_2 and CO_2 and then compared to numerical solutions. Through computational analysis and criteria relative to gas turbine operation, they determined that the flame temperature must be lower than 1273 K after dilution for material resistance reasons. They found that about 60% of cold CO_2 by volume would be necessary to cool the flue gases lower than the 1273 K limit[19].

Daniele et. al have studied the turbulent flame speed for syngas-air at gas turbine conditions. To test the experiments, a high-pressure combustor was designed and is capable of operation up to 20 bar and inlet temperature of 773 K with a maximum thermal power of 400 kW. The combustion chamber has a length of 12.6 in and an inner diameter of 2.9 in. The combustor is made of double wall quartz tubes that are air-cooled. No more details are given about the design.

They found that the ratio of turbulent flame velocity and laminar speed is highly dependent of preferential diffusive thermal effects and that it is much higher for syngas than for methane[20].

The University of California Irvine Combustion Laboratory (UCICL) has two pressure vessels that can operate up to 15.2 bar pressure and inlet temperatures up to 922 K. The first vessel has a high optical access and full traversing, which allows for detailed in-situ measurements. The second vessel has a smaller optical access and is designed for long duration tests for durability evaluations. The second facility is also capable of measuring emissions and flame stability. A control facility can provide up to 1 kg/s of air and can supply liquid fuel and natural gas. Natural gas can be supplied at 0.09 kg/s at 34.5 bar. This fuel supply is equivalent to 4.5 MW of thermal power input. Extensive laser diagnostics can be done on both test rigs. However, it is not specified if the facilities can operate with oxygen instead of air. Details about the design of the vessels or operation and control systems are also not specified[21].

Princeton University has a high-pressure chamber capable of pressures up to 30 bar. The combustor can use gas fuels as well as light and heavy liquid fuels. The chamber consists of two concentric cylindrical vessels with diameters of 100 mm and 280 mm. The length of the combustion chamber is 152.4 mm. It has optical access through a quartz window. The pressure was kept constant by using magnetic controlled pressure release door. Studies performed with this test rig found that flame speed decreases substantially with increasing pressure. Possible diagnostics include temperature measurements and a digital particle image velocimetry (DPIV) for fluid velocity measurements[22], [23].

Cambridge University has a high-pressure combustion facility able to operate with pressures up to 10 bar and can supply preheated air up to 873 K with a mass flow rate of 0.09 kg/s. The combustor also has an optical access window. The combustion chamber is 200 mm long and has an inner diameter of 135 mm. It is cooled down by flowing air between the quartz tube and the surrounding pressure vessel. The pressure is controlled by a variable area flow restrictor. The combustor is used mainly for liquid fuels but can also accommodate gaseous fuels. Possible optical diagnostics include planar laser induced fluorescence (PLIF), laser doppler anemometry (LDA),

particle dynamics anemometer (PDA), and particle image velocimetry (PIV). The research focuses on flame structure, soot formation, and thermoacoustics at turbine operating conditions[24][25].

The Georgia Institute of Technology has done studies of flame flashback and lean blowout characteristics at pressures of up to 4.5 bar and inlet temperatures of 470 K. The combustor is optically accessible by using a quartz tube with 76 mm diameter quartz tube housed inside a pressure vessel. The studies found that hydrogen compositions of less than 60% have a reduced effect on flashback characteristics than blowout[26].

Pennsylvania State University has a High Pressure Combustion Laboratory focused on studying gaseous, solid, liquid, and gelled propellants for rockets and propulsion systems. A high-pressure strand burner with optical access that can operate at pressures of up to 9000 psi (620 bar) is used for solid propellant characterization. An ultra-high pressure strand burner can deliver compressed gases at pressures approaching 30,000 psi (2068 bar)[27].

The DLR Institute of Combustion in Germany has developed the high-pressure combustor rig Stuttgart (HBK-S) that can supply 1.3 kg/s of air at 40 bar and 1000 K. It can use natural gas and other gaseous and liquid fuels with a maximum thermal power input of 2 MW. The facility can measure pressure, temperature, flow rates, and emissions as well as extensive optical diagnostics[28].

The literature review reveals that there are numerous existing test rigs used for the study of high pressure combustion. However, information available regarding the design of the high-pressure combustion chambers, thermal management, burners, and feed system are very limited. Another point that stands out is that all the facilities found in the literature use air as the oxidizer. The design presented in this thesis will use oxygen as the oxidizer and will implement a burner design made with additive manufacturing.

2.2 – UTEP High Pressure Combustion

The HPC at UTEP was originally designed to operate with a thermal power input of 500 kW and a chamber pressure of up to 15 bar. It was designed to study flames with varying concentrations of syngas, a gas composed of a combination of CO and H_2, and using air as the oxidizer. The combustion chamber was designed using these parameters and was able of withstanding adiabatic flame temperatures of 2400 K for test durations of 30 seconds maximum[24], [25], [29], [30]. All of the combustor if made of SS410. The following sections will go over each component of the existing HPC, which consist of: 1) inlet manifold, 2) front cap, 3) combustor body, 4) exit cap, and 5) control system. Figures 3.1 and 3.2 illustrate the different sections of the HPC.

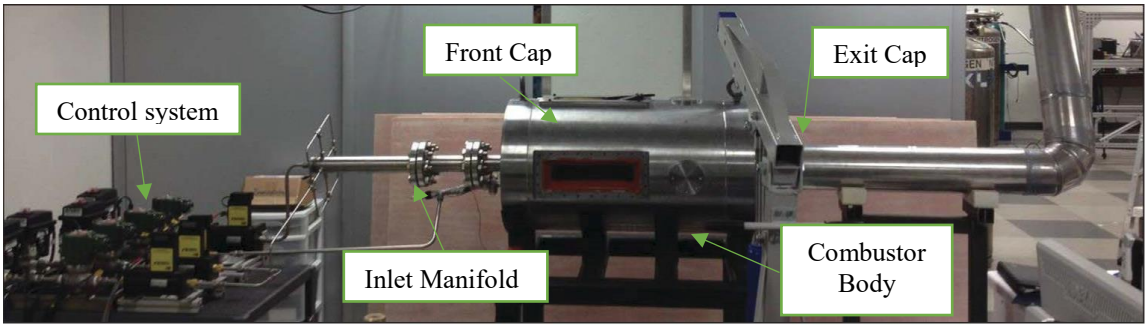

Figure 2.1 – Previous HPC design.

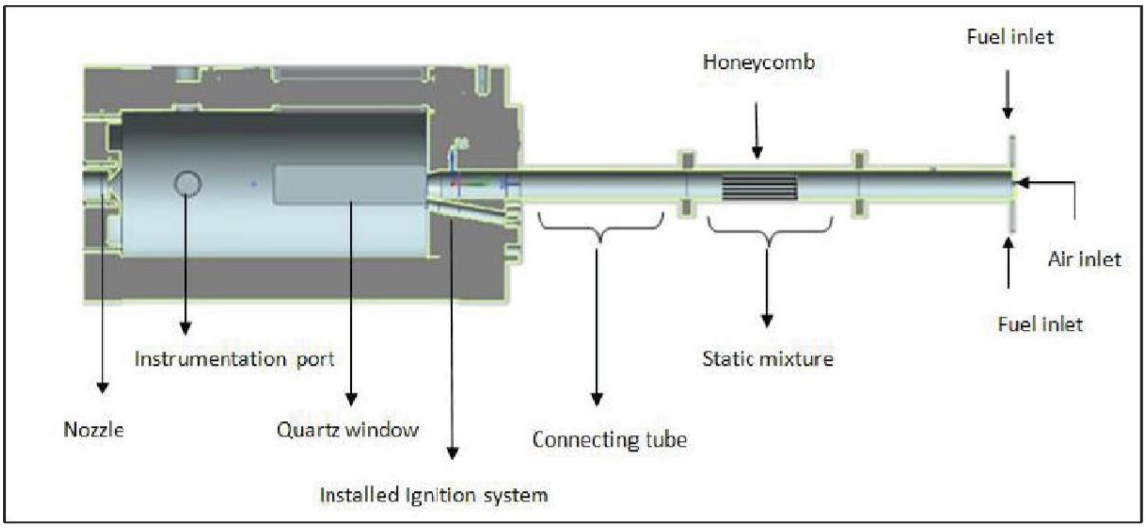

Figure 2.2 – Half section view of previous HPC design.

2.2.1 – Inlet manifold

The HPC was designed to operate with a lean-premixed combustion process. The inlet manifold, displayed in Figure 3.3, is the section before the combustion chamber where the fuel and air mix and it is made of 3 parts: 1) injection section, 2) static mixer, and 3) combustor connector. The first section of the manifold is the mixing section. Here, the air is injected to a tube and the fuel is injected through four ports normal to the air flow direction. This aids the fuel and air to mix properly, leading to a better combustion process.

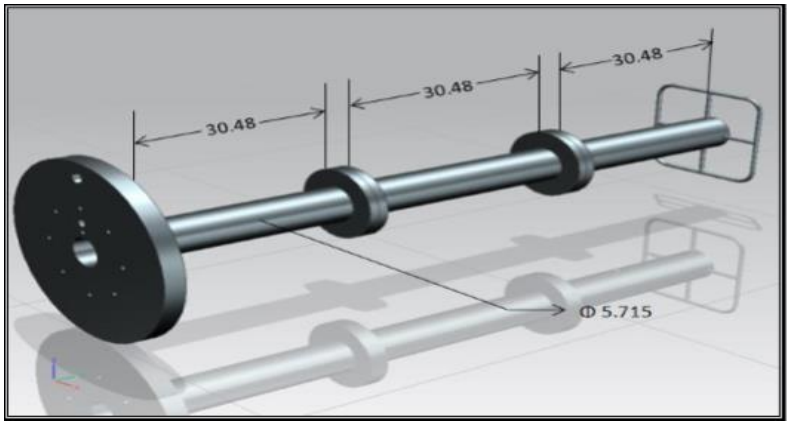

Figure 2.3 – Full assembly of inlet manifold. Dimensions in cm.

The second section of the inlet manifold is the static mixer. This section is composed of a 3-D printed honeycomb structure inside the tube and can be seen in Figures 3.4 and 3.5. The purpose of the static mixer is to eliminate flow irregularities induced from the injection of the fuel and air and improve laminar flow. The third section of the inlet manifold is the part that connects the manifold to the front cap.

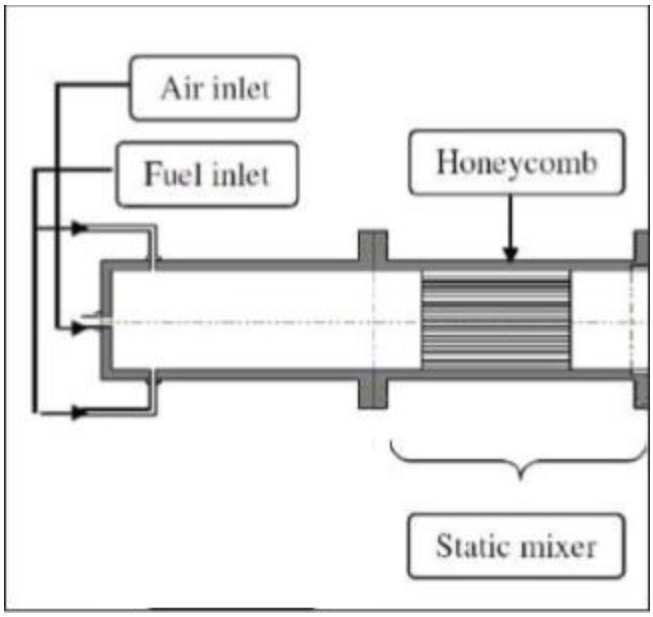

Figure 2.4 – Cross section view of the first two sections of the inlet manifold.

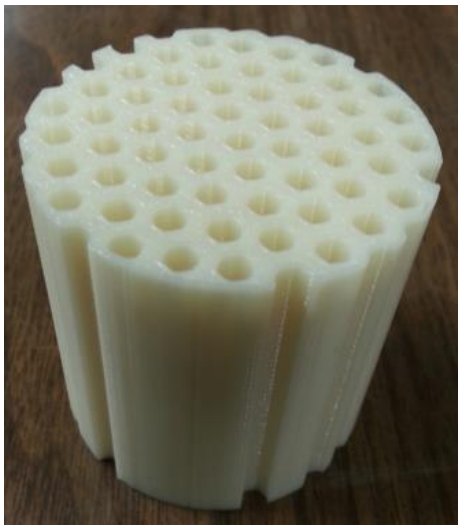

Figure 2.5 – 3D Printed honeycomb static mixer.

2.2.2 – Front Cap

The front cap is what connects the inlet manifold to the combustor body. It also houses the swirler or multi-tube injector, and igniter. Since the project was previously used to experiment flashback and blowout propensity as well as emissions analysis, the front cap was designed so that either a swirler or a multi tube injector could be used to mix the fuel and oxidizer. Each of them

having advantages and disadvantages. Figure 3.6 shows the front view of the front cap as well as a transparent side view where the swirler or multi-tube port can be seen at the center and the angled port below it is for the igniter.

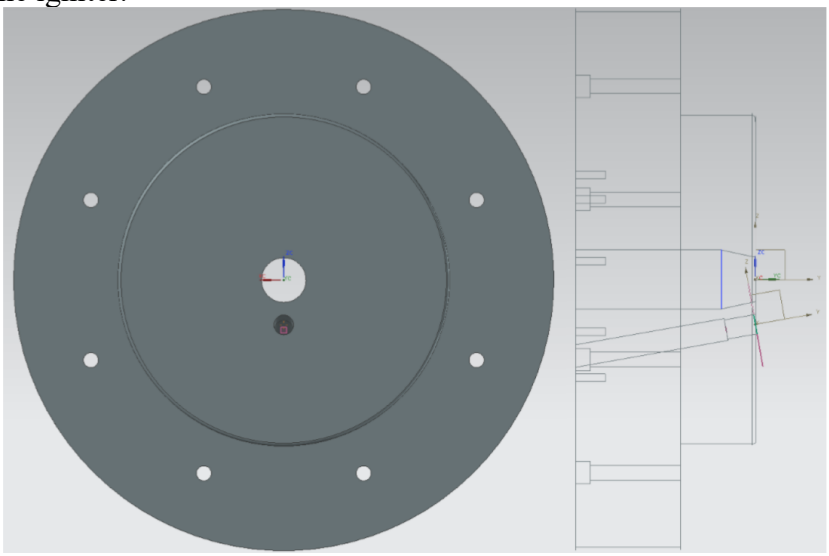

Figure 2.6 – Previous front cap design.

2.2.2.1 – Swirl burner

The swirl burner has a center body made of stainless steel and 12 vanes made of anodized aluminum. It has a swirl number of 0.97 that has been shown to have an effect on flame size, shape, stability, and combustion intensity. The swirler used can be seen in Figure 3.6.

Figure 2.7 – Swirler used to mix fuel and oxidizer gases.

2.2.2.2 – Multi-tube Injector

The multi-tube injector (MTI) was designed to operate with high-hydrogen concentration of fuel gases. Its purpose is to increase the stability of syngas flames and to reduce pollutant emissions when compared to a swirl burner. The MTI was designed with thirteen 4 mm diameter orifices distributed along the injector head and is also made of SS 410. The orifices at the center are 7 mm apart while the orifices at the perimeter are 10 mm apart. The assembly of the MTI can be seen in Figure 3.8.

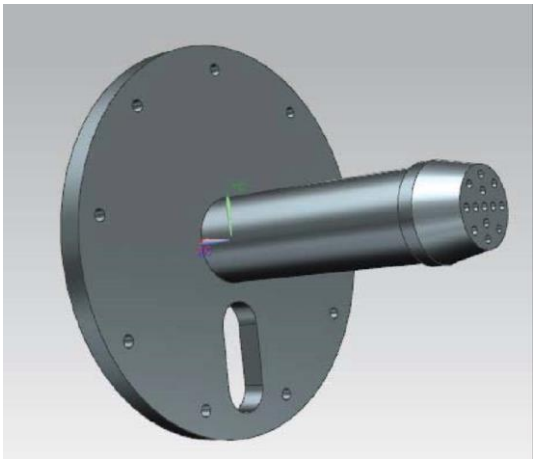

Figure 2.8 - Multi-tube injector for high hydrogen fuel concentrations.

2.2.2.3 – Igniter

The igniter consists of a modified spark plug where a rod of Haynes 230 with a length of 45.7 cm was welded to a spark plug. It was necessary to increase the length of the spark plug to get it inside of the combustor. A casing of two concentric tubes was designed for the igniter that allowed methane and air to be fed into the combustion chamber. However, these gases were not premixed. It was also necessary to insulate the Haynes 230 rod so that the spark could be carried to the tip of the electrode. Methane and air were fed into the combustion chamber and ignited with the modified spark plug, creating a diffusion flame that was used to ignite the main injector. Figure 3.9 shows the igniter components and Figure 3.10 shows the assembly of the igniter mounted to the front cap.

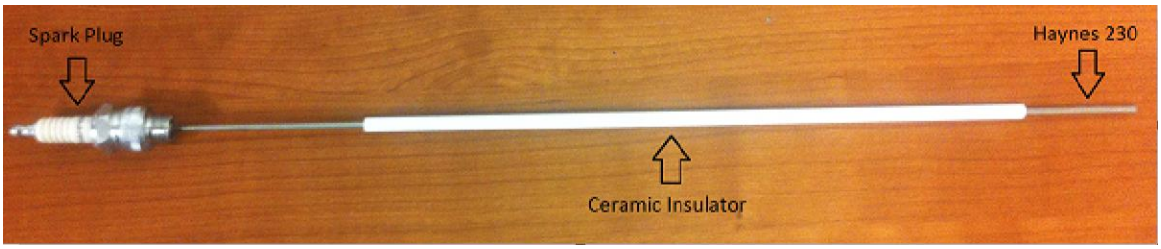

Figure 2.9 – Spark plug components.

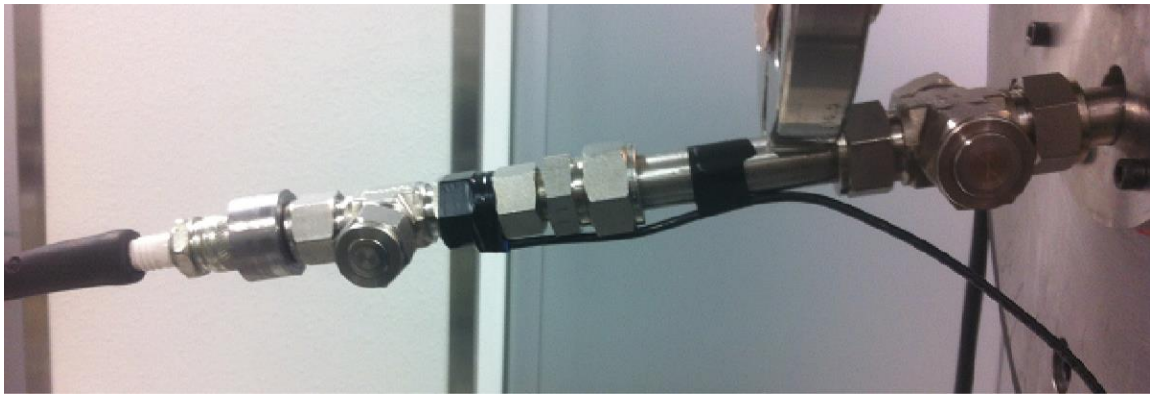

Figure 2.10 – Spark plug assembly.

2.2.3 – Combustor Body

The body of the combustor is made of SS 410. It was determined through an iterative process using finite element analysis software that the necessary wall thickness had to be 3.5 inches to withstand the temperature load and the pressure load. It has an outer diameter of 18 in, an inner diameter of11 in, and a length of 25.5 in. The maximum stress was found to be 355 MPa while the minimum yield strength of SS 410 is 575 MPa. The maximum stress points were found to be at the edges of the windows and of the instrumentation ports due to the change in geometry and thus resulting in stress concentration zones. The body of the combustor has three 31.75x10.16 cm quartz windows for optical access located at both sides and at the top of the combustor. Instrumentation ports are circular with a diameter of 5.08 cm and are also located at the both sides and the top of the combustor. However, the instrumentation ports were not used and were left only as covers.

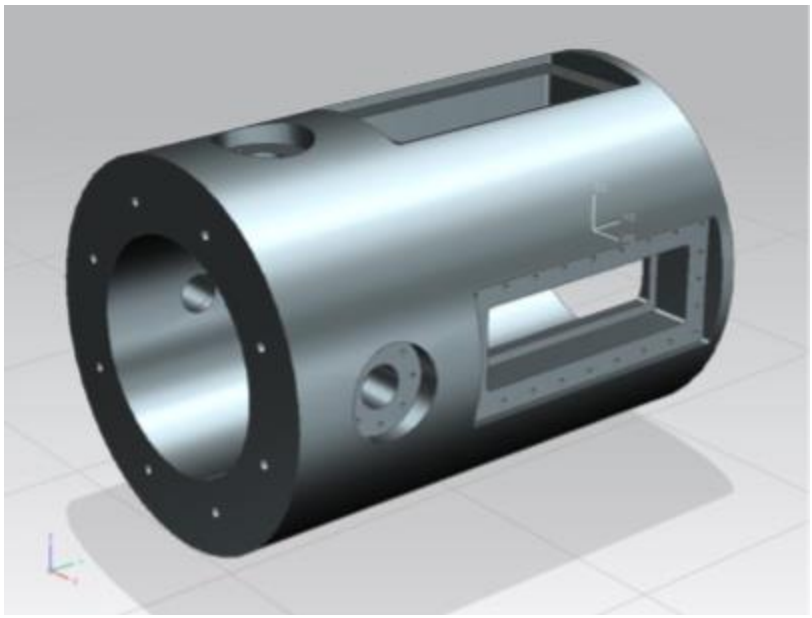

Figure 2.11 – CAD of combustor body.

2.2.4 – Exit Cap

The exit cap consists of two modular sections. The first part is the cap that connects to the combustor body and the second part is a converging nozzle that is used to control the pressure inside the combustion chamber. The exit cap also has a diameter of 18 inches and is fastened to the combustor body using eight 0.5 in bolts. The exit nozzle area was calculated to be 161.3 mm^2 which is equal to a hole with a diameter of 14.3 mm. The exit nozzle is bolted to the exit cap from the inside and the attachment holes can be seen on Figure 3.12.

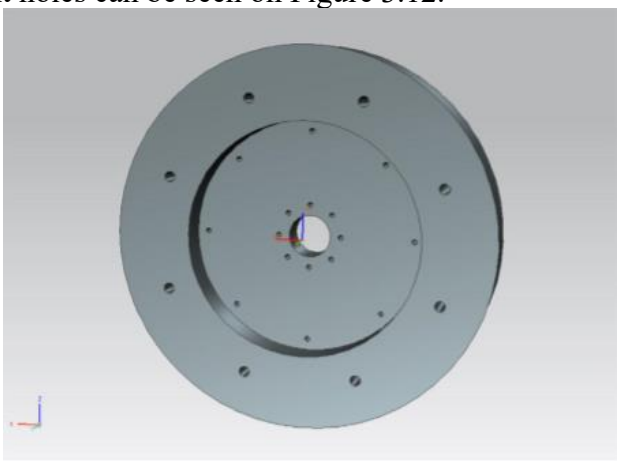

Figure 2.12 – CAD of previous exit cap.

Figure 2.13 – Machined exit nozzle.

2.2.5 – Control System

The system was designed to be controlled from a remote location using LabView and the schematic can be seen in Figure 3.14. The LabView program was able to control proportional flow valves, used to regulate the flow during testing. Next are needle valves, which were used as a manual safety precaution after system shut down and ensure that there would be no flow in case of defective proportional valves or solenoid valves. The solenoid valves were also controlled remotely with LabView to open or close the flow in each line. Flow meters were used to measure the amount of mass flow going through each line and confirm that the desired amount was being delivered. The flow meters reading could be monitored through LabView in the control room. Pressure transducers were used in each line to measure the gas pressure going into the combustor and their readings could also be monitored from the control room. The ignition system consisting of a modified spark plug could also be controlled remotely with LabView. Finally, a manual shut off system was implemented in case of an emergency.

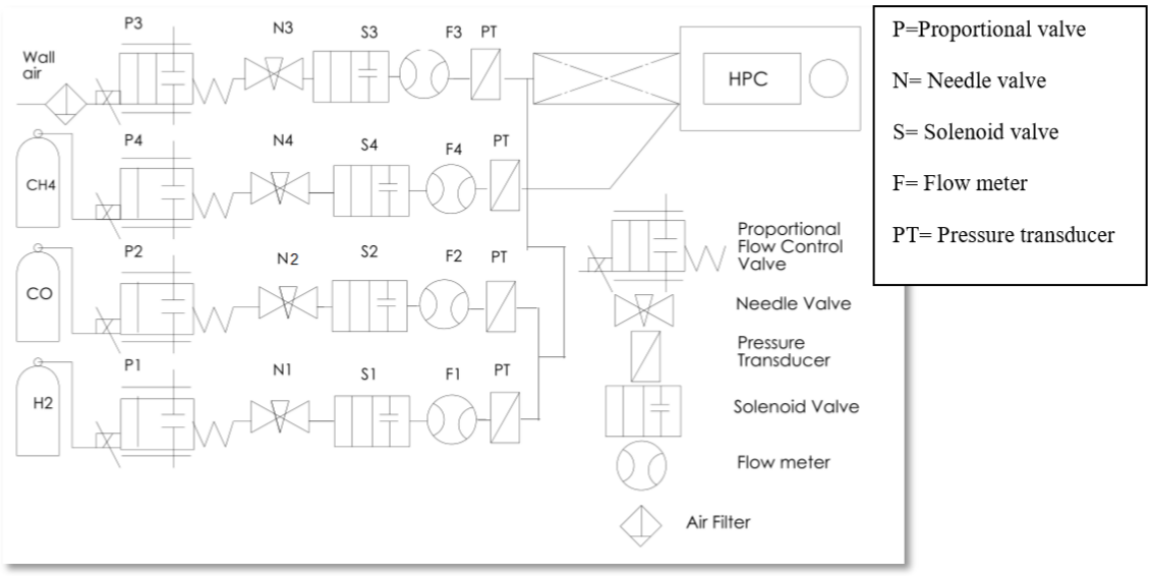

Figure 2.14 - Previous feed system schematic.

Chapter 3: Design Methodology

3.1 – New Design Requirements

The design requirements for the high-pressure combustor are:

1. Thermal power input: Up to 500 kW
2. Fuel and Oxidizer: Oxygen and Methane
3. Operating Pressure: 20 bar
4. Test duration: Up to 2 hours
5. Fuel mixture: Stoichiometric

3.2 – Flow Rates Calculation

The first step was to calculate the necessary mass flow rates of methane and oxygen. The fuel mas flow rate can be defined as the thermal power input divided by the lower heating value (LHV) of the fuel as shown in Equation 1. The lower heating value is used because it is assumed that the water product from the combustion process is vapor. Knowing that the thermal power is 500 kW and that the lower heating value of methane is 50,016 kJ/kg, the result yields a mass flow rate of 0.01 kg/s of methane[31]. The stoichiometric oxidizer to fuel ratio of oxygen and methane is 4 and can be calculated using Equation 3 and is defined as two times the molecular weight (MW) of oxygen (32 g/mol) over the molecular weight of methane (16 g/mol). Finally, the mass flow rate of oxygen can be calculated using Equation 2. This calculation yields a mass flow rate of 0.04 kg/s for oxygen. Therefore, the total mass flow rate of fuel and oxidizer is 0.05 kg/s.

$$\dot{m}_{CH_4} = \frac{Thermal\ Power\ Input}{LHV_{CH_4}} \tag{1}$$

$$\dot{m}_{O_2} = \dot{m}_{CH_4} * \left({}^{O}/_{F}\right)_{stoic.} \tag{2}$$

Where,

$$\left({}^{O}/_{F}\right)_{stoic} = 2 * \left(\frac{MW_{O_2}}{MW_{CH_4}}\right) \tag{3}$$

3.3 – INJECTORS

Chowdhury et. al have designed the injectors and the summary is presented in this section[32]. Shear co-axial injectors were designed to deliver the necessary thermal power input of 500 kW. This type of injector has two concentric tubes where one of the tubes feeds the fuel and the other feeds the oxidizer at a different velocity. It utilizes the shear forces between the fuel and oxidizer to mix. These shear forces are driven by the momentum flux difference between the two streams. As shown in Figure 3.1, methane is fed through the center and oxygen is fed through the bigger tube surrounding it. Cooling passages were also implemented to maintain the face of the injector cool. Two thermocouple ports are used to measure the temperature of the face, where the wall thickness from the tip of the probe to the combustion chamber is 3 mm. The injectors were made using additive manufacturing electron beam melting (EBM). Due to the use of this technique, the injector was designed specifically to be able to be printed.

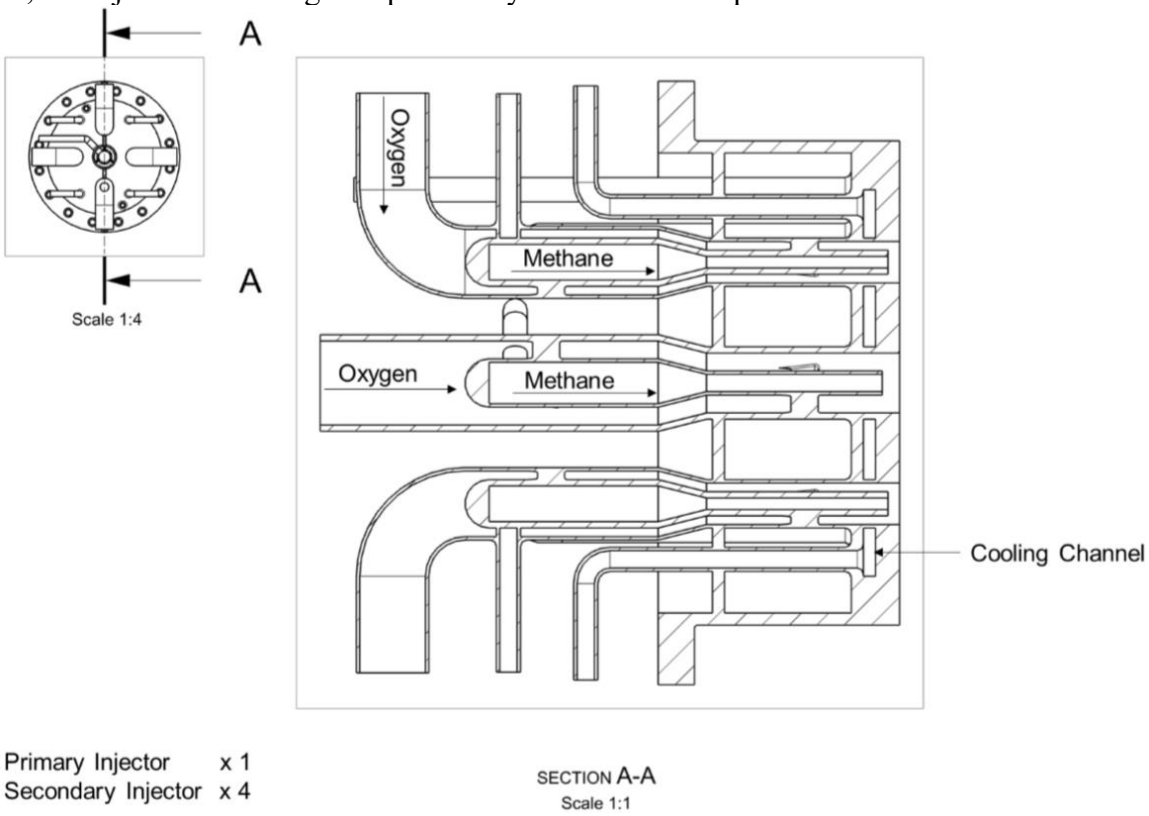

Figure 3.1 – Shear co-axial injector cross-sectional view.

To design the shear co-axial injectors and ensure proper mixing, two non-dimensional parameters, velocity ratio (VR) and momentum flux ratio (J) are used. Equations 4 and 5 show how to calculate each of these parameters[33].

$$VR = \frac{v_{CH_4}}{v_{O_2}} \tag{4}$$

$$J = \frac{\rho_{CH_4} * v_{CH_4}^2}{\rho_{O_2} * v_{O_2}^2} \tag{5}$$

There is a total of 5 shear co-axial injectors to divide the total power input. The primary injector is at the center and the 4 smaller injectors surrounding it are referred to as secondary injectors. The detailed breakdown of power inputs, mass flowrate, velocity flowrates and momentum flux ratios are shown in Table 3.1. The step-down geometry of the injectors is to create a pressure drop across the line, which is thought to assist in preventing the flame from propagating inside the line i.e. flashback.

Table 3.1 – Injector parameters

	Primary Injector	Secondary Injector (each)
Power Input (kW)	40 - 200	15 - 75
CH_4 mass flowrate (g/s)	0.8 - 4	0.3 - 1.5
O_2 mass flowrate (g/s)	3.2 - 16	1.2 - 6
CH_4 velocity (m/s)	3.5 - 18	3.5 - 17
O_2 velocity (m/s)	0.75 - 3.5	0.75 - 3.5
Momentum flux ratio	≈12	≈12

The primary injector and secondary injectors are designed with turn down ratios of 5. The velocity and momentum flux ratios are kept constant for both the primary and secondary injectors. Typical values for momentum flux ratio for shear coaxial injectors varies between 2 to 25[33]. Furthermore, a small recess of the center post enhances the combustion performance[33]–[36]. For example, Kendrick et al. found that a recess of 1di, where 'di' represents high velocity jet diameter, in LOx/H_2 combustion increases the flame expansion rate and width of the flame volume[34]. Tripathi et al. investigated that the increment of momentum flux ratio or recess length enhances

the jet breakup. The authors have also found that the effect of recess length is higher when the momentum flux ratio is small[35]. However, it has been demonstrated that increasing the recess length above 1.5di does not further improve the combustion performance. Another study, by Wheeler and Kirby, found that a recess length close to 1.3di in LOX/CH_4 combustion further enhances combustion efficiency[36]. For the proposed injector, the recess length of 1di is used, Fig. 3.2.

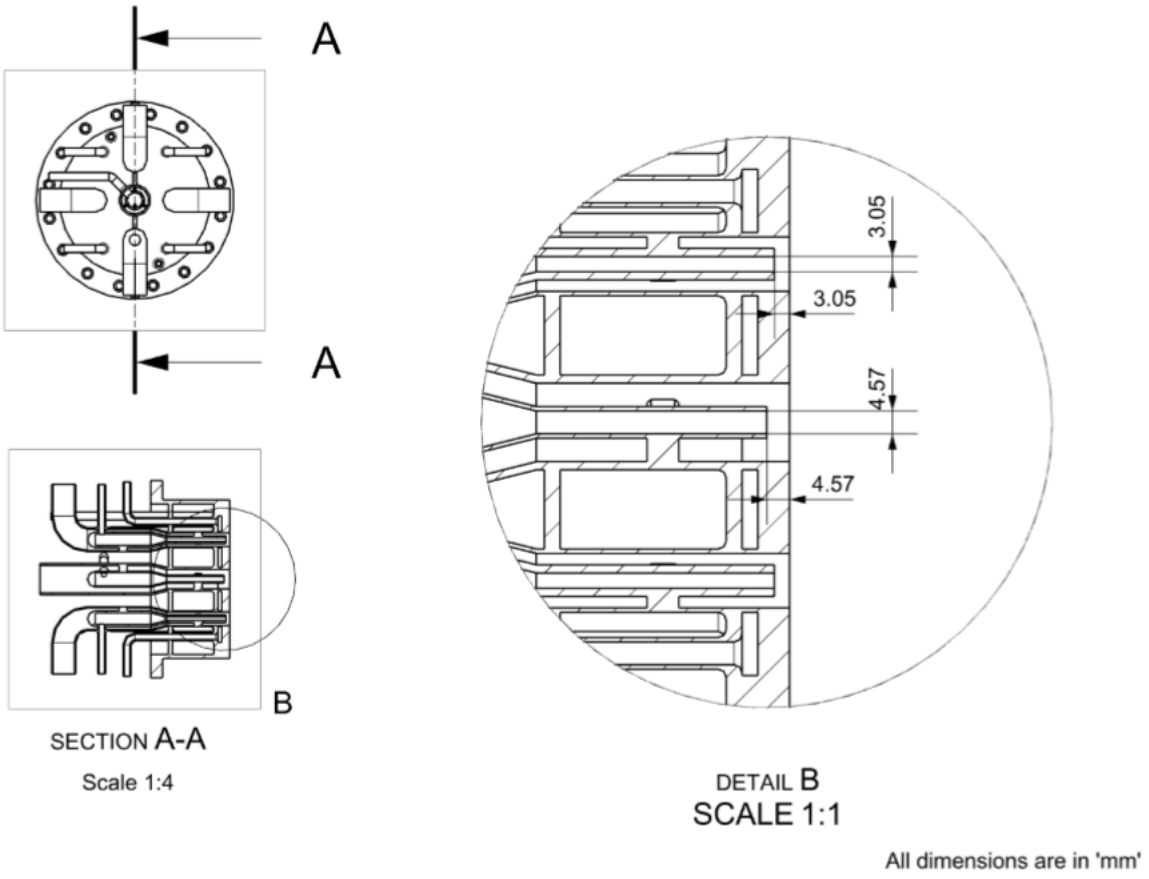

Figure 3.2 – Injector recess length

3.4 – Adiabatic Flame Temperature

The adiabatic flame temperature is the theoretical maximum temperature that the flame will reach during the combustion process. To calculate the adiabatic flame temperature, NASA's

Chemical Equilibrium with Applications (CEA) software was used[37]. A constant pressure solver was used with inputs of operating pressure (20 bar), fuel and oxidizer used (gaseous methane and oxygen), inlet temperature (room temperature), and equivalence ratio. CEA calculated that at the given operating conditions, the adiabatic flame temperature would be 3500 K. This temperature is significantly higher than what the HPC was originally designed. The previous tests done with a syngas and air composition had an adiabatic flame temperature of 2200 K. The rise in temperature is a result of using oxygen instead of air as the oxidizer. In a typical air combustion process, the air is composed of roughly 77% nitrogen and 23% oxygen by mass fraction. However, nitrogen doesn't combust and mainly serves as a heat sink, reducing the flame temperature[31]. Lower adiabatic flame temperatures and shorter firing periods allowed the combustor to operate safely without any cooling in previous tests, but due to the new requirements it was necessary to perform a thermal analysis to check if a cooling solution would be needed. An example of the code used for NASA CEA can be found in the appendix.

3.5 – Wall Temperature

The next step was to establish the requirements of the cooling system to be used with the combustor. The project requirement of a 2-hour continuous fire was equivalent to the assumption of a steady state operation. To prove the need for additional cooling, the inner wall temperature was calculated. The NASA CEA program run previously to determine the adiabatic flame temperature also outputs other important gas parameters that can be used for the calculation of the inner wall temperature. Equations (4)-(6) were used to determine the convective heat transfer coefficient inside the combustion chamber[38]. The assumptions for these calculations are that the combustion process is complete, the product gases are evenly mixed, the flow is fully developed, and that there is no recirculation of the gases.

$$Re = \frac{\rho V D}{\mu} \tag{6}$$

$$Nu = \frac{\left(f/8\right) Re\ Pr}{1.07 + 12.7\left(f/8\right)^{0.5}\left(Pr^{2/3} - 1\right)} \quad (7)$$

$$h = \frac{Nu\ k}{D} \quad (8)$$

Where Re is the Reynolds number, ρ is the density of the combustion gases, V is the gas velocity, μ is the gas dynamic viscosity, Nu is the Nusselt number, Pr is the Prandtl number of the combustion gases, f is friction factor, h is the convective heat transfer coefficient, k is the thermal conductivity of the gas, and D is the hydraulic diameter. After calculating the convective heat transfer coefficient of the hot gas side, a 2-D thermal resistance model was used to calculate the combustion chamber's inner wall temperature. The calculation yielded a temperature of 3120 K. Therefore, it was concluded that a cooling solution had to be implemented for the material to withstand the temperature, as the maximum continuous operating temperature from the manufacturer is 800ºC. A sample calculation can be found in the appendix as well as material properties.

3.6 – Structural Analysis

Rios et. al have done the structural analysis of the HPC and the summary is presented in this section[39]. The combustion chamber of the HPC will be subject to two main sources of stress. The first one is a mechanical stress caused by the pressure inside the combustor trying to push the walls outwards. The second is a thermal stress caused by the temperature gradient between the inner walls containing the combustion and the outer walls exposed to the environment. Knowing that the inner pressure would be constant at 20 bar, the task was to find the maximum allowable temperature so that the sum of the mechanical and thermal stresses was lower than the material yield strength at the expected operating temperature.

3.6.1 – Analytical Analysis

The combustor body has an outer radius of 0.23 m (9 in) and an inner diameter of 0.14 m (5.5 in), giving a wall thickness of 0.9 m (3.5 in). When the ratio of mean radius to wall thickness

is less than 10, it has to be treated as a thick wall. Solving Eq. 9 yielded a ratio of 2, thus it was determined that the combustor body could be treated as a thick-walled cylinder. Therefore, Eq. 10 was used to determine the hoop stress due to pressure for a thick-walled pressure vessel. Solving Eq. 10 yielded a hoop stress of 4 MPa when the inside pressure was 20 bar and the outside pressure was 1 atm.

$$W = \frac{r_{mean}}{wall\ thickness} \tag{9}$$

$$\sigma_{hoop} = \frac{r_i^2 P_i - r_o^2 P_o}{(r_o^2 - r_i^2)} + \frac{(P_i - P_o) r_i^2 r_o^2}{(r_o^2 - r_i^2) r_i^2} \tag{10}$$

The thermal stress was calculated using Eq. 11[40].

$$\sigma_{th} = \frac{E \alpha q t}{2(1-v)k} \tag{11}$$

Where, E is the Young's Modulus of SS 410, α is the coefficient of thermal expansion of SS 410, q is the heat flux, t is the thickness of the combustor, υ is Poisson's ratio of SS 410, and the k is the thermal conductivity of SS 410.

The basic equation for heat flux is:

$$q = \frac{k\left(T_{wg} - T_{wair}\right)}{t} \tag{12}$$

By substituting Eq. 12 into Eq. 11, the resulting thermal stress equation becomes:

$$\sigma_{th} = \frac{E \alpha \left(T_{wg} - T_{wair}\right)}{2(1-v)} \tag{13}$$

Since the modulus of elasticity and the coefficient of thermal expansion are dependent on temperature, the thermal stress result is also dependent on temperature. Furthermore, the material yield strength also depends on temperature and decreases as it rises[41]. To find the maximum

allowable operating temperature inside the combustion chamber, the total stress, consisting of the sum of the mechanical and thermal stress, and the material yield strength were plotted as a function of temperature, Figure 3.3.

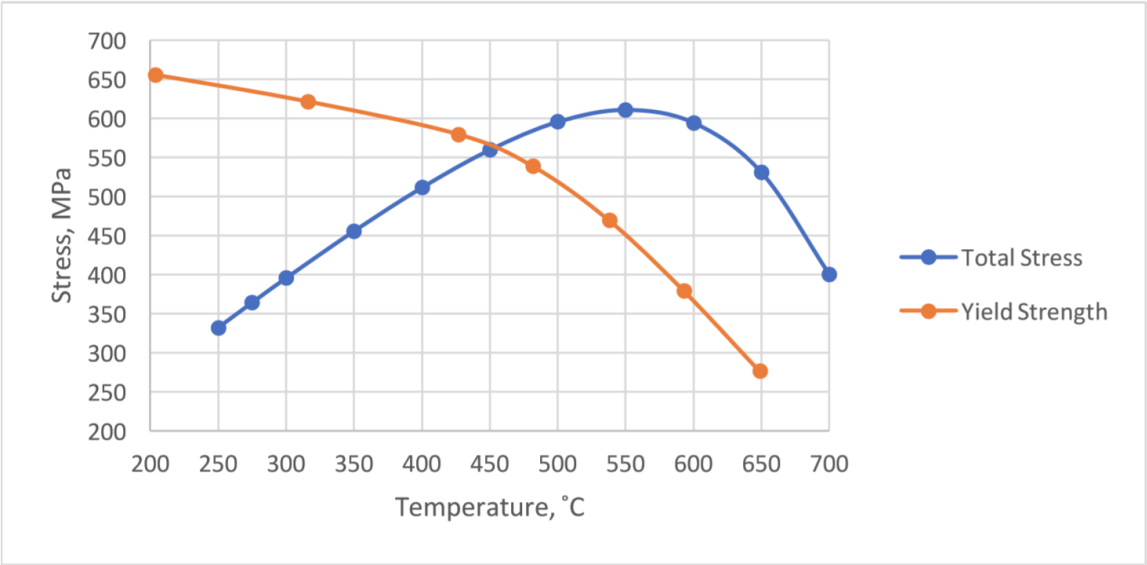

Figure 3.3 – Total stress and yield strength vs temperature[39].

The plot shows that failure is expected to occur if the temperature of the inner walls exceeds 450 °C. Therefore, a factor of safety of 1.4 was selected, corresponding to a maximum allowable inner wall temperature of 315 °C or ≈600 K.

3.6.2 – Numerical Analysis

The use of a commercial Finite Element Analysis (FEA) software was used to determine the maximum allowable inner wall temperature to avoid material failure. The software used was ANSYS Mechanical. The material properties of SS 410 were input into the software material parameters taking into account their temperature dependence[41].

A simplified geometry of the combustor body was modeled and due to its symmetry, only one quarter had to be modeled to be representative of the whole combustor body. This approach helped reduce the computing time to find results. To simulate the mechanical and the thermal stresses acting on the combustor body, a coupled simulation was used.

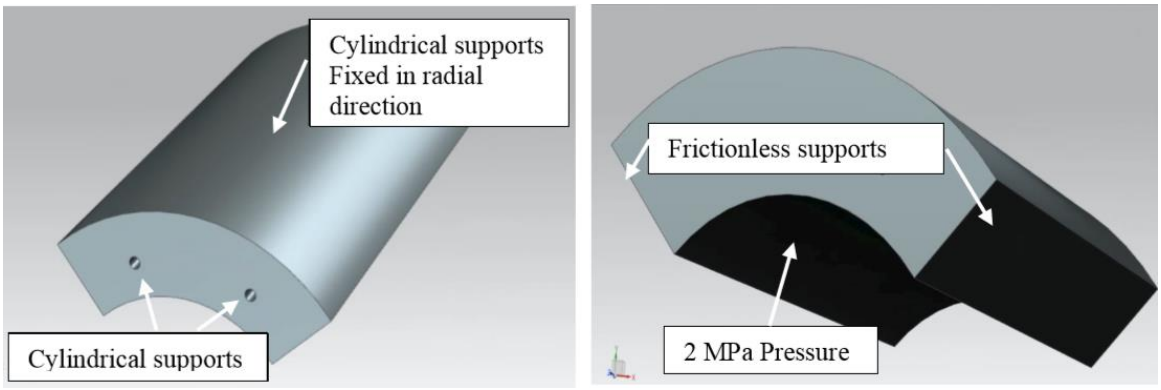

Figure 3.4 – Boundary conditions used in the FEA model[39].

For the thermal stress, a steady state solver was used. Due to the long test duration of 2 hours, this model is valid. For the inner walls, a constant temperature of 700 °C was set as well as convection. For the outer walls, convection was also used with an ambient temperature of 25 °C. For the mechanical stress, the supports used are shown in Fig. 3.4. A uniform pressure of 20 bar was applied normal to the inner surface going outwards. A pressure of 1 atm was applied to the outer surface going inwards.

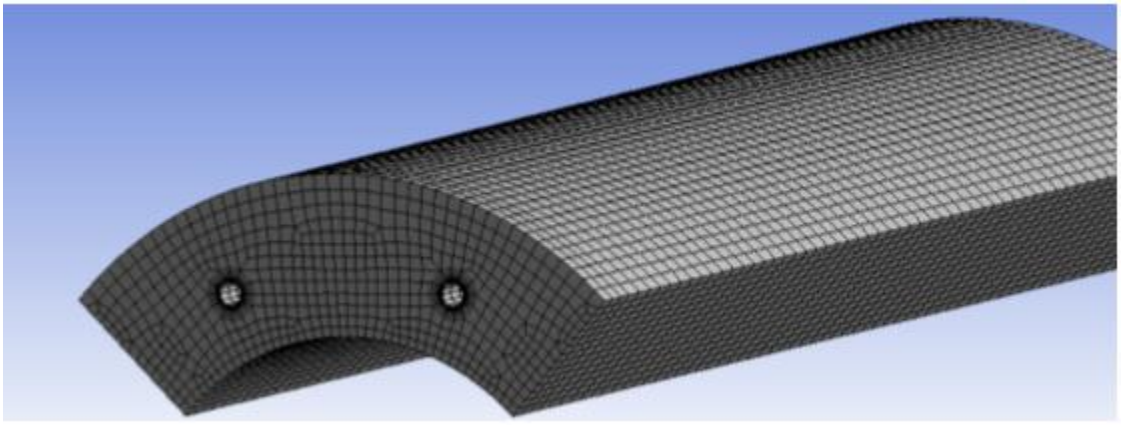

Figure 3.5 – Mesh used for the FEA simulation of the combustor body[39].

The mesh has a total of 48,800 elements and 208,780 nodes that are refined around the bolt holes. A summary of the mesh metrics is shown in Table 3.2

Table 3.2 – Mesh metrics for 3D FEA model.

Nodes			48,800	
Elements			208,780	
Mesh Metric	Min	Max	Average	Standard Deviation
Element Quality	1.60E-2	0.999	0.608	0.345
Aspect Ratio	1.024	125.88	13.963	1.1581
Jacobian Ratio	1.0012	159.53	1.2372	2.5416
Orthogonal Quality	0.568	0.999	0.964	6.598E-2
Skewness	7.71E-3	.665	0.133	0.117

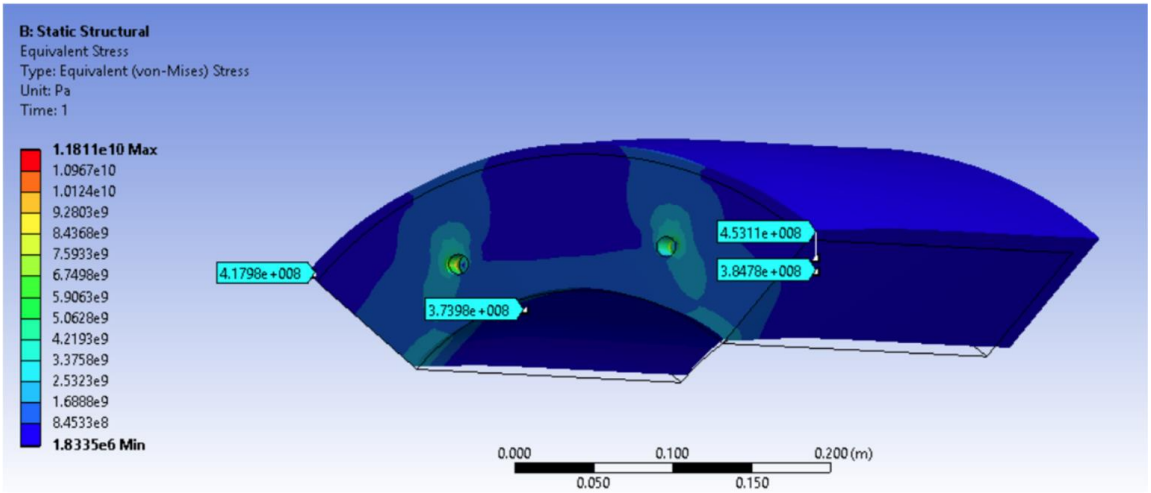

Figure 3.6 – Equivalent Von-Mises stress results[39].

The scale in Fig. 3.6 show a maximum value of the stress of 845 MPa instead of the 400 MPa the analytical solution yielded. This is due to the addition of axial and radial stress in the simulation, which wasn't considered in the analytical analysis. Other points were probed as seen in Fig 4.6 and the average stress is 407 MPa. This is only a 2% error from the analytical results of 400 MPa.

3.7 – Thermal Analysis

When methane and oxygen combust, the residuals, assuming complete combustion, are water and carbon dioxide. As mentioned earlier, in a typical oxy-combustion power generation system, the water is condensed and the CO_2 is recirculated into the combustion chamber. For this reason, CO_2 was selected to be used for cooling since it could be obtained from the combustion

flue gases. Another factor that influenced this decision was the high cost associated to modifying the combustor body to implement water cooling.

The first option that was explored was to dilute the gases with CO_2. The added carbon dioxide would absorb heat released from the combustion process and reduce the flame temperature. Due to the possibility of blowing off the flame by adding CO_2, the maximum flow of CO_2 was limited to 50% by volume. Since the methane and oxygen mass flow rates were fixed, and would be injected at room temperature and at a pressure of 20 bar, the volumetric flow rate of those gases could be calculated. Afterwards, Equation 14 was used to calculate the volumetric flow rate of CO_2 in the gas dilution mixture and Equation 15 was used to calculate the mass flow of CO_2. The corresponding volumetric flow rates and mass flow rates of CO_2 can be seen in Table 3.3. A sample calculation con be found in the appendix.

$$\dot{V}_{CO_2} = \left[\frac{\left(\dot{V}_{CH_4} + \dot{V}_{O_2}\right)(Desired\ \%)}{100 - Desired\ \%}\right] \tag{14}$$

$$\dot{m}_{CO_2} = \dot{V}_{CO_2} * \rho_{CO_2} \tag{15}$$

Table 3.3 – Mass flow rates of CO_2 at different dilution percentages.

% CO_2 by Volume	**CO_2 Massflow (kg/s)**
0% CO_2	0
5% CO_2	0.00
10% CO_2	0.01
15% CO_2	0.02
20% CO_2	0.02
25% CO_2	0.03

30% CO_2	0.04
35% CO_2	0.05
40% CO_2	0.06
45% CO_2	0.07
50% CO_2	0.09
55% CO_2	0.11
60% CO_2	0.14
65% CO_2	0.17
70% CO_2	0.21
75% CO_2	0.27
80% CO_2	0.36

After calculating the mass flow rates of CO_2, NASA's CEA program was used again to calculate the adiabatic flame temperature with increasing CO_2 dilution. The results can be seen in Figure 3.7.

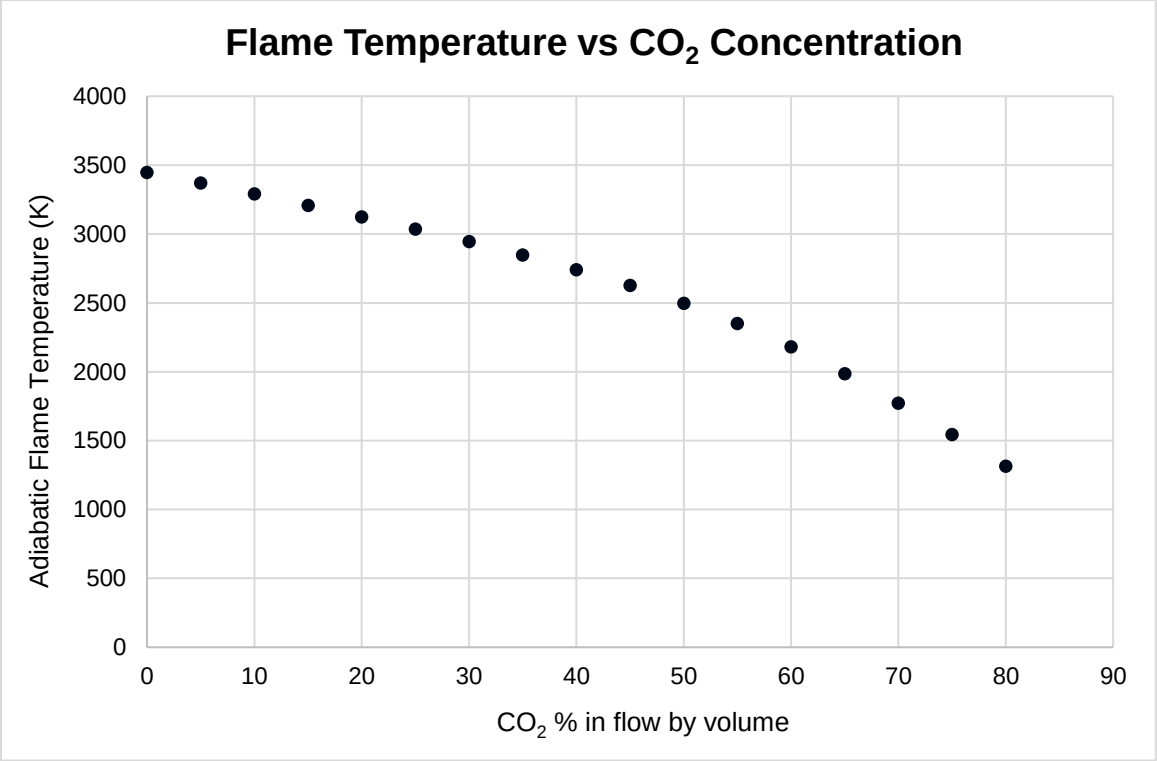

Figure 3.7 – Adiabatic flame temperature vs % CO_2.

It was found that by diluting the gas mixture with CO_2, the adiabatic flame temperature would still be too hot to safely operate the combustor for long duration tests. Therefore, to meet the cooling requirements, a high velocity ring of CO_2 was injected along the inner walls of the combustion chamber. In this configuration CO_2 acted as a protective layer, keeping the walls at the maximum allowable temperature of 600 K. The numerical analysis will be presented on Chapter 4 and the final design on Chapter 5.

3.8 – THROAT DIAMETER

The exit of the combustor has a reduced area that acts as a nozzle. The purpose of the area reduction is to maintain the pressure inside the combustion chamber at 20 bar. To calculate the exit area, Equations 16 and 17 were used. Equation 16 demonstrates that the flow will be sonic at the throat due to the pressure difference inside and outside of the combustor. Afterwards, Equation 17 can be used to calculate the necessary throat area only when it is known that the flow will be choked. The parameters used in these equations were obtained from NASA CEA using 50% CO_2

by volume. The assumption is that the all the gases are evenly mixed and at a constant temperature by the time they reach the exit nozzle. The calculations yield a throat diameter of 10.4 mm. A sample calculation can be found in the appendix.

$$\frac{P_c}{P_1} = \left(\frac{2}{k+1}\right)^{\frac{k}{k-1}} \tag{16}$$

$$A_{throat} = \frac{\dot{m}_{total}}{\sqrt{k\rho P_1 \left(\frac{2}{k+1}\right)^{\frac{k+1}{k-1}}}} \tag{17}$$

$$D_{throat} = \sqrt{\frac{4 * A_{throat}}{\pi}} \tag{18}$$

Where Pc is the critical pressure, if the pressure outside the combustion chamber is lower than the critical pressure, the flow will be choked. P_1 is the chamber pressure, k is the specific heat ratio of the gases, m dot is the total mass flow rate (which includes methane, oxygen, and $CO_{2)}$, ρ is the density of the gases, A_{throat} is the area at the throat, and D_{throat} is the diameter at the throat.

3.9 – IGNITER

The injector will be ignited using a pilot flame. This pilot flame will be provided by an igniter design previously made at UTEP by Sanchez et. al [42]. The igniters were developed to serve as the ignition source for 500 lb and 2000 lb thrust engines and use a swirl injection system, Fig. 3.8. The igniters were also designed to be used with methane and oxygen, which are already needed for the injector. The igniter consists of four main parts: 1) igniter body, 2) inlet valves, 3) in-line orifices, and 4) spark ignition system. The design is compact enough that it can be fit into the existing circular instrumentation ports of the combustor body. Two igniters will be used to start the injector, one on the left and on the right side of the combustor.

Figure 3.8 – Torch igniter design[42].

Chapter 4: Numerical Methodology

To accurately model the 500 kW HPC, it was necessary to define the problem with the conditions of operation. This meant having a steady-state simulation with compressible flow and non-premixed gases. To simulate and solve this problem, ANSYS FLUENT, a commercial numerical solver, was used. FLUENT is capable of calculating the heat transfer, chemical reactions, and gas dynamics of the combustion process. The governing equations used by this software package will be demonstrated here[43].

4.1 – Continuity and Momentum Conservation Equations

For 2D axisymmetric geometries, the continuity equation is solved by:

$$\frac{\partial \rho}{\partial t} + \frac{\partial}{\partial x}(\rho v_x) + \frac{\partial}{\partial r}(\rho v_r) + \frac{\rho v_r}{r} = S_m \tag{19}$$

The conservation of momentum is solved by:

$$\frac{\partial}{\partial t}(\rho \vec{v}) + \nabla \cdot (\rho \vec{v}\vec{v}) = -\nabla p + \nabla \cdot (\bar{\bar{\tau}}) + \rho \vec{g} + \vec{F} \tag{20}$$

Where the stress tensor is:

$$\bar{\bar{\tau}} = \mu \left[(\nabla \vec{v} + \nabla \vec{v}^T - \frac{2}{3} \nabla \cdot \vec{v} I \right] \tag{21}$$

Table 4.1 – Continuity and momentum equation variables.

Symbol	Description
ρ	Density
t	Time
v_x	Axial velocity
v_r	Radial velocity
r	Radial coordinate
x	Axial coordinate
$\vec{v}$	Velocity vector
p	Static pressure

$\bar{\bar{\tau}}$	Stress tensor
$\rho\vec{g}$	Gravitational body force
$\vec{F}$	External body force
μ	Molecular viscosity
I	Unit tensor

4.2 – ENERGY EQUATION

The energy equation for non-premixed non-adiabatic combustion model is used. In this case, FLUENT uses the total enthalpy form of the energy equation and assumes that the Lewis number (Le) = 1. The Lewis number is defined as the ratio of thermal diffusivity to mass diffusivity and is utilized when there is simultaneous heat and mass transfer in a fluid flow. Under this assumption, the conduction and species diffusion terms combine to give the first term on the right-hand side of Eq. 22. The contribution from viscous dissipation appears in the non-conservative form as the second term on the right-hand side.

$$\frac{\partial}{\partial t}(\rho H) + \nabla \cdot (\rho \vec{v} H) = \nabla \cdot \left(\frac{k_t}{c_p}\nabla H\right) + S_h \tag{22}$$

Where the total enthalpy is defined as:

$$H = \sum_j Y_j H_j \tag{23}$$

And the total enthalpy of a species is defined as:

$$H_j = \int_{T_{ref,j}}^{T} c_{p,j}\, dT + h_j^0\left(T_{ref,j}\right) \tag{24}$$

Table 4.2 – Energy equation variables.

Symbol	**Description**
H	Total enthalpy
ρ	Density
$\vec{v}$	Velocity vector
k_t	Turbulent thermal conductivity

c_p	Specific heat
S_h	Heat of chemical reaction and specified volumetric heat sources
Y_j	Mass fraction of species j
H_j	Total enthalpy of species j
$h_j^0(T_{ref,j})$	Formation enthalpy of species j at the reference temperature $T_{ref,j}$

4.3 - TURBULENCE

The k-epsilon turbulence model is used in most general purpose CFD codes and is considered an industry standard due to its proven stability, numerical robustness, and well established predictive capability. To model turbulence in the flow, FLUENT uses the Standard k-epsilon model, which solves two transport equations. The turbulent kinetic energy is given by Eq. 25 and its dissipation rate is given by Eq. 26.

$$\frac{\partial}{\partial t}(\rho k) + \frac{\partial}{\partial x_i}(\rho k u_i) = \frac{\partial}{\partial x_j}\left[\left(\mu + \frac{\mu_t}{\sigma_k}\right)\frac{\partial k}{\partial x_j}\right] + G_k + G_b - \rho\varepsilon - Y_M + S_k \qquad (25)$$

$$\frac{\partial}{\partial t}(\rho \varepsilon) + \frac{\partial}{\partial x_i}(\rho \varepsilon u_i) = \frac{\partial}{\partial x_j}\left[\left(\mu + \frac{\mu_t}{\sigma_\varepsilon}\right)\frac{\partial \varepsilon}{\partial x_j}\right] + C_{1\epsilon}\frac{\varepsilon}{k}(G_k + C_{3\varepsilon}G_b) - C_{2\varepsilon}\rho\frac{\varepsilon^2}{k} + S_\varepsilon \qquad (26)$$

Table 4.3 – Turbulence equation variables.

Symbol	**Description**
ρ	Density
k	Kinetic energy
x_i	Position on i
u_i	Velocity on i
x_j	Position on j
μ	Viscosity
μ_t	Turbulent viscosity
σ_k	Turbulent Prandtl number for k
σ_ε	Turbulent Prandtl number for ε
G_k	Turbulence kinetic energy due to mean velocity gradients

G_b	Turbulence kinetic energy due to buoyancy
ε	Dissipation rate of kinetic energy
Y_M	Contribution of the fluctuating dilation in compressible turbulence to the overall dissipation rate
S_k , S_ε	User-defined source terms
$C_{1\epsilon}$, $C_{2\varepsilon}$, $C_{3\varepsilon}$	Constants

4.4 – NON-PREMIXED COMBUSTION

Since the methane, oxygen and carbon dioxide would be injected from individual ports, the non-premixed model was used to estimate the gas characteristics. The model simplifies the thermochemical state of the fluid into a single scalar quantity known as mixture fraction, Eq. 27. This model predicts the local mass fraction of burnt and unburnt fuel stream elements in all the species, in other words combustion is simplified to a mixing problem. A probability density function (PDF) estimates the fraction of time that the fluid is close to the mixture fraction value. A PDF table is calculated beforehand for a given the given fuel, oxidizer, and secondary stream. Density and temperature are calculated depending of the mixture fraction at a point

$$f = \frac{Z_i - Z_{i,ox}}{Z_{i,fuel} - Z_{i,ox}} \tag{27}$$

When a secondary stream (carbon dioxide in our case) is introduced, the sum of the three mixture fractions in the system is always equal to 1.

$$f_{fuel} + f_{sec} + f_{ox} = 1 \tag{28}$$

Table 4.4 – Mixture fraction equation variables.

Symbol	**Description**
Z_i	Elemental mass fraction for element i
$Z_{i,ox}$	Mass fraction of oxidizer stream inlet
$Z_{i,fuel}$	Mass fraction of fuel stream inlet
f_{fuel}	Fuel mass fraction
f_{sec}	Secondary stream mass fraction
f_{ox}	Oxidizer mass fraction

4.5 – GEOMETRICAL ADAPTATION FOR 2D MODEL

The primary injectors of methane and carbon dioxide were able to me modeled without any change using the symmetry plane because they are the center. However, the secondary injectors of both fuel and oxidizer, as well as the CO_2 inlet ports had to be modified to fit the 2D geometry. In a 2D axisymmetric model, the geometry revolves around a plane to create the 3D model. Since the secondary injectors and CO_2 injectors are individual circles, they had to be modified to create rings with the same area. To mimic the secondary shear co-axial injectors, 3 concentric rings were created, where the middle ring was methane and the ring outside and inside were oxygen. Using the mass conservation equation and leaving the distance from the center of the combustor to the center of the inlet ports constant, a ring configuration was calculated that had the same total area, mass flow, velocity, and density. Using this method to adapt the geometry was beneficial to reduce the computation time and iterate the design faster. A sample calculation can be found in the appendix.

$$\dot{m}_1 = \dot{m}_2 \tag{29}$$

$$\rho_1 A_1 v_1 = \rho_2 A_2 v_2 \tag{30}$$

Where $\dot{m}$ denotes the mass flow rate, ρ is fluid density, A is cross sectional area of inlet port, and v is the velocity of the fluid. Since the density and velocity were kept constant, only the area term was manipulated to create the 2D axis-symmetric geometry, Fig 4.1.

The fluid domain after the throat section was used as the exit with a pressure of 1 bar. It was necessary to do this to let FLUENT solve for the chamber pressure depending on the throat area restriction. If the fluid domain was set where the throat ends, the pressure input would force FLUENT to find a solution for the specified exit pressure, independent of the hole size. This would give erroneous velocity and pressure results.

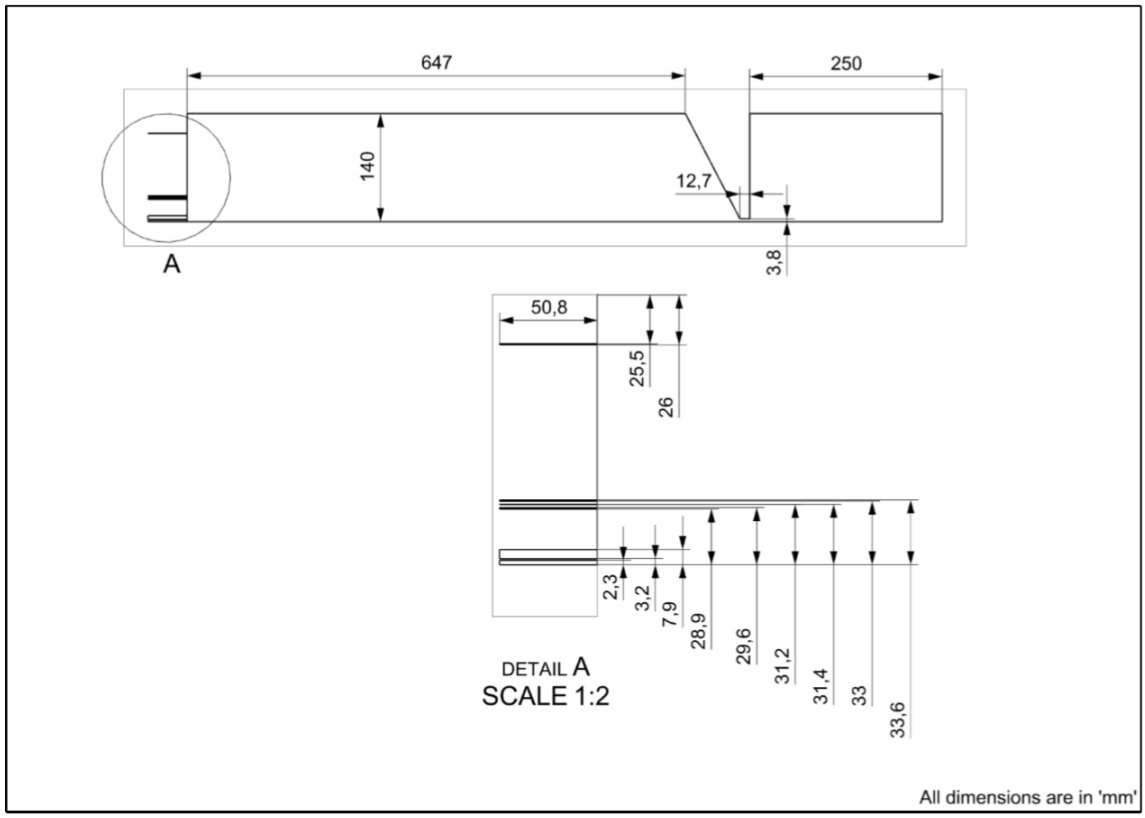

Figure 4.1 – Fluid domain for 2D model[32].

4.6 – MESH

A mesh was created using ANSYS's built in mesh manager. The mesh is created prior to setting the boundary conditions and is necessary for the program to run. The mesh divides the geometry into smaller sections. Ideally, the sections are as close to a square or an equilateral triangle in shape as possible, depending on the chosen element type. Having the ideal shape helps the solution to be more accurate, if the boundary conditions are set correctly. For this reason, it is important to know the mesh metrics to evaluate the mesh quality. The summary of the mesh metrics for the mesh used is shown in Table 5.5. The mesh metrics showed that the mesh was of good quality and would yield realistic results.

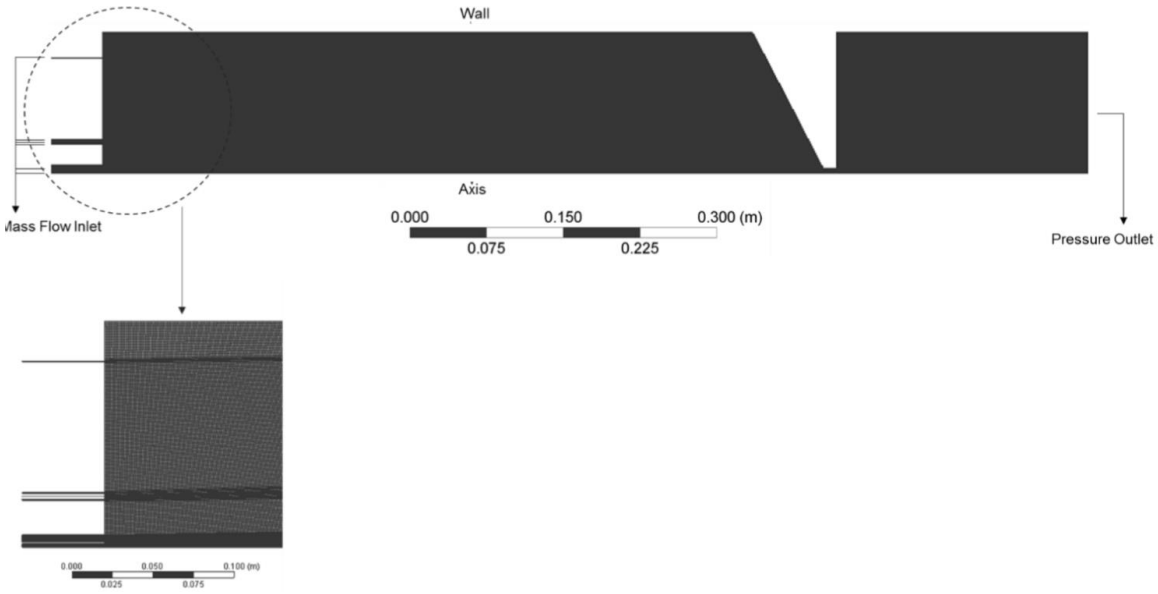

Figure 4.2 – 2D Axisymmetric mesh.

Table 4.5 – Mesh metrics for 2D CFD model.

Nodes		45778		
Elements		44024		
Mesh Metric	Min	Max	Average	Standard Deviation
Element Quality	6.57E-2	0.999	0.839	0.169
Aspect Ratio	1.000	29.208	1.52	1.1581
Jacobian Ratio	1	4.300	1.003	2.47E-2
Orthogonal Quality	0.629	1.000	0.970	3.598E-2
Skewness	1.30E-10	.613	0.110	0.108

4.7 – BOUNDARY CONDITIONS

The boundary conditions employed for this model are summarized in Table 4.6

Table 4.6 – Boundary Conditions used on 2D model.

General Solver	• Type: Pressure-Based • Velocity Formulation: Absolute • Time: Steady • 2D Space: Axisymmetric
Models	• Energy: On

	• Viscous Model: standard k-epsilon, standard wall functions
	• Radiation: P1
	• Species: Non-Premixed Combustion
	  o Inlet Diffusion: On
	  o Compressibility: On
	  o Fuel stream rich flammability limit: 0.23
	  o Secondary stream rich flammability limit: 1

Materials	• PDF Mixture • Stainless Steel

Boundary Conditions	• Fuel Inlet: Mass-flow-inlet (CH_4)
	  o Primary: 0.004 kg/s
	  o Secondary: 0.006 kg/s
	  o Temperature: 300 K
	• Oxidizer Inlet: Mass-flow-inlet (O_2)
	  o Primary: 0.016 kg/s
	  o Secondary: 0.012 kg/s (each)
	  o Temperature: 300 K
	• Secondary stream: Mass-flow-inlet (CO_2)
	  o Total: 0.09 kg/s
	  o Temperature: 300 K
	• Pressure Outlet: 1 bar

Solution Methods	• Scheme: Coupled • High order term relaxation
Solution Initialization	• Hybrid Initialization

Chapter 5: Results and Discussion

5.1 – 2D CFD Results

The first model run in FLUENT was for a 500 kW thermal power input with 0.09 kg/s of CO_2 injected along the walls of the combustor. For this model, the end cap geometry was left with the original exit diameter of 2 in. The results demonstrated that the inner walls of the HPC would exceed the maximum allowable operating temperature of 600 K, Fig. 5.1. The CO_2 stream was only effective for ¼ of the length of the combustor and the remainder would heat up beyond the temperature safety limit. This was attributed to a gas recirculation zone towards the exit of the combustor. Recirculation of the hot gases was observed because of the geometry of the combustor. The straight end cap wasn't helping the gases flow smoothly towards the exit area.

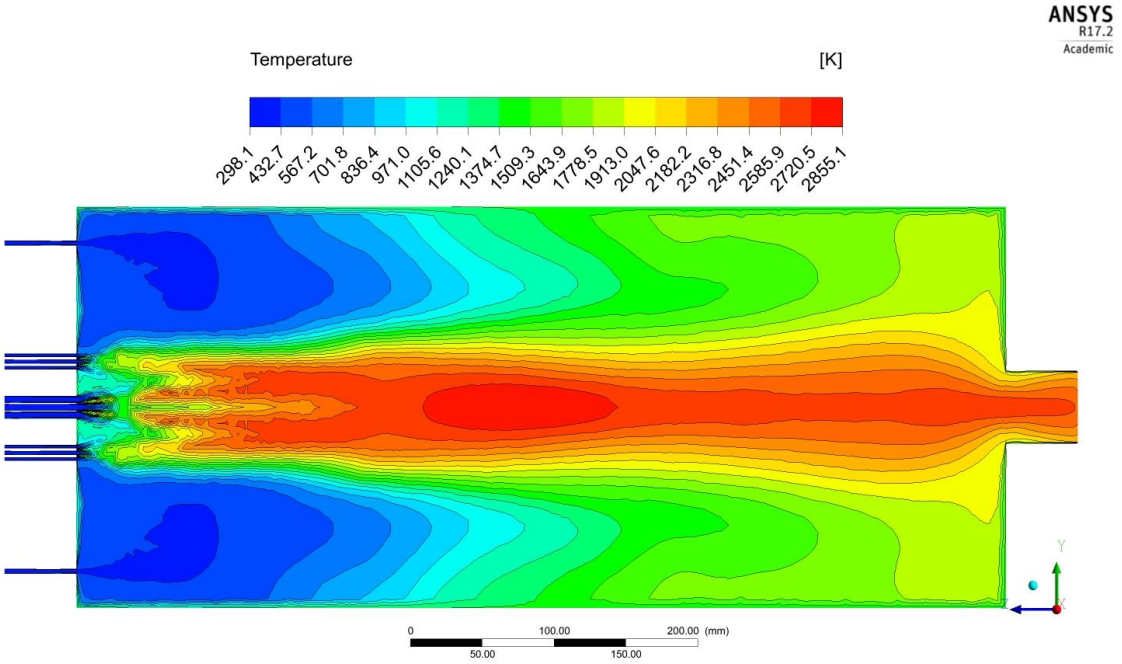

Figure 5.1 – Temperature contours of the HPC with a straight face exit, diameter of 2in.

To resolve the issue of the recirculating gases near the exit of the combustion chamber, it was proposed to make a new exit cap that was angled. By angling the end, the gases would flow

towards the exit area and the recirculation zone would be minimized. This approach proved to be successful and lower temperatures were observed along the combustion chamber. Figure 5.2 shows the temperature contour of the HPC with an exit of 27.5° from vertical. In this case, the CO_2 stream is much more effective at shielding the inner walls from the hot combustion gases and keeping the walls at a safe temperature. The CO_2 stream effectively keeps the inner walls at or below 600 K for ¾ of the combustor's length. However, it is observed that the inlet section at the injector face and the exit portion of the combustion chamber are still exceeding the maximum allowable temperatures. To cool these sections, water cooling channels were implemented into the design of the injector face and of the new exit cap plates. Alternatively, if more cooling is needed, the windows located near the exit of the combustor will be capable of supplying a secondary stream of CO_2.

An exit angle of 45° was also tested but it did not significantly reduce temperatures compared to the 27.5°case. In addition, due to the increased cost, weight, and cooling requirements associated with the use of this size cap the 27.5° case was selected instead.

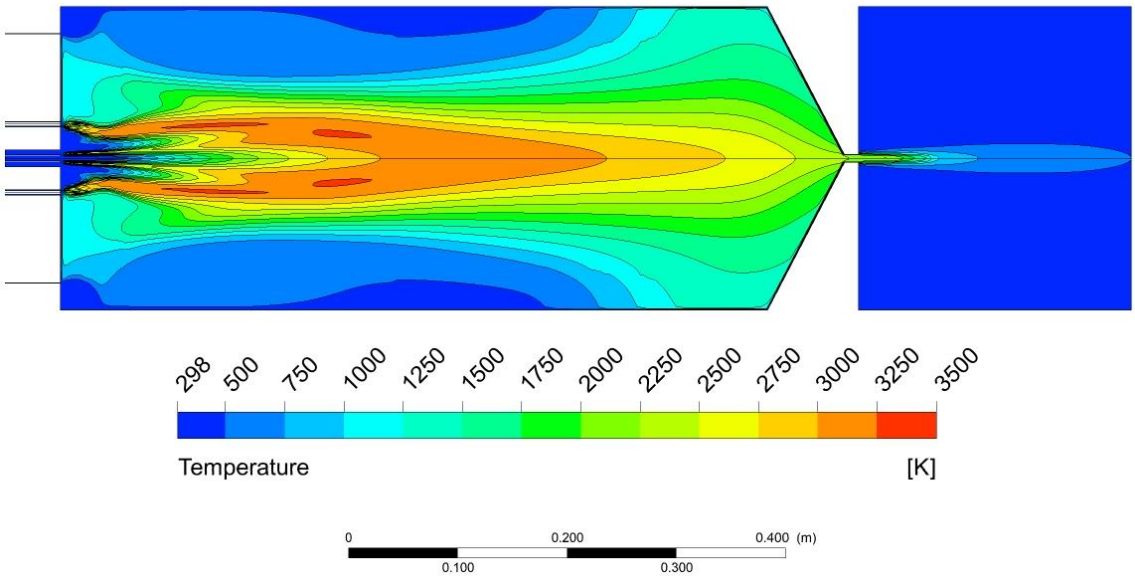

Figure 5.2 – Temperature contour of HPC with 27.5° exit.

Figure 5.3 shows the path lines inside the combustion chamber. Two recirculation zones can be observed at the beginning of the combustor. The zone closest to the walls is primarily CO_2 at low temperatures, thus not affecting wall temperatures in this region. The zone closest to the center of the combustor is composed of a mixture of hot gases and CO_2. The temperature isn't as hot as the adiabatic flame temperature but is hot enough for the injector face to require active water cooling.

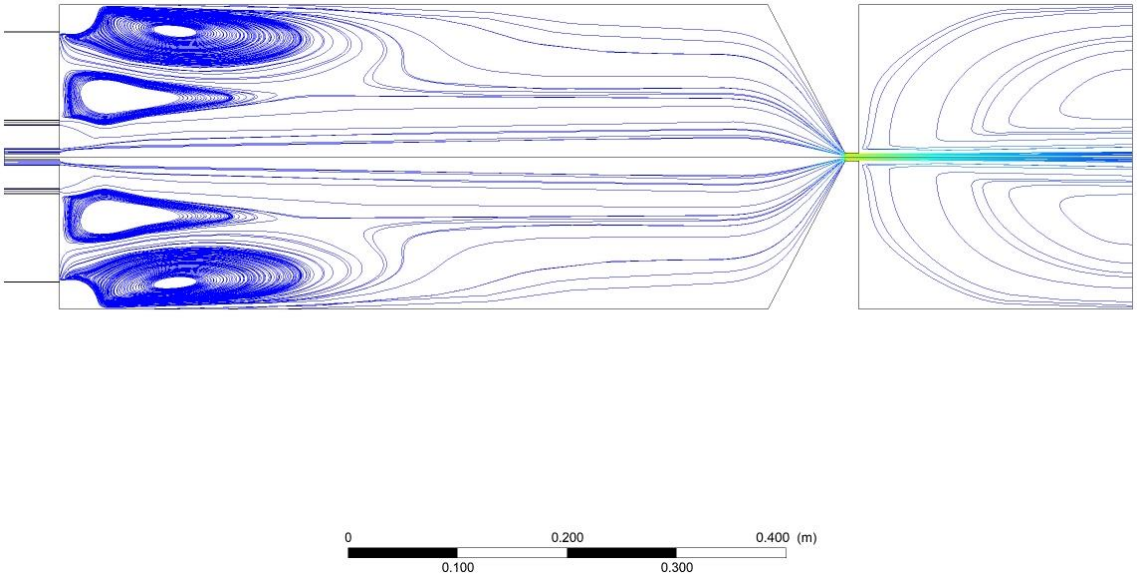

Figure 5.3 – Path lines of fluid flow inside the combustion chamber.

The pressure contour shown in Fig. 5.4 demonstrates the combustion chamber will reach the required pressure of 20 bar. However, through iterations it was found that a throat diameter of 7.6 mm would pressurize the chamber to 20 bar in FLUENT.

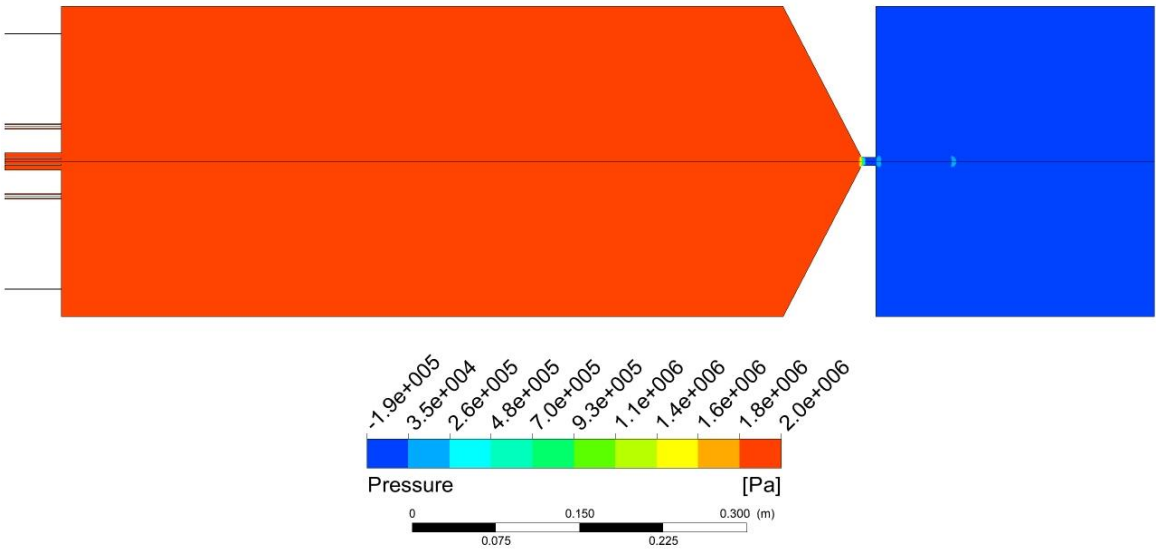

Figure 5.4 – Pressure contour of HPC with nozzle exit.

The velocity contours are shown in Fig. 5.5, this confirms that the flow will reach sonic velocity at the throat section, as stated by the critical pressure calculation.

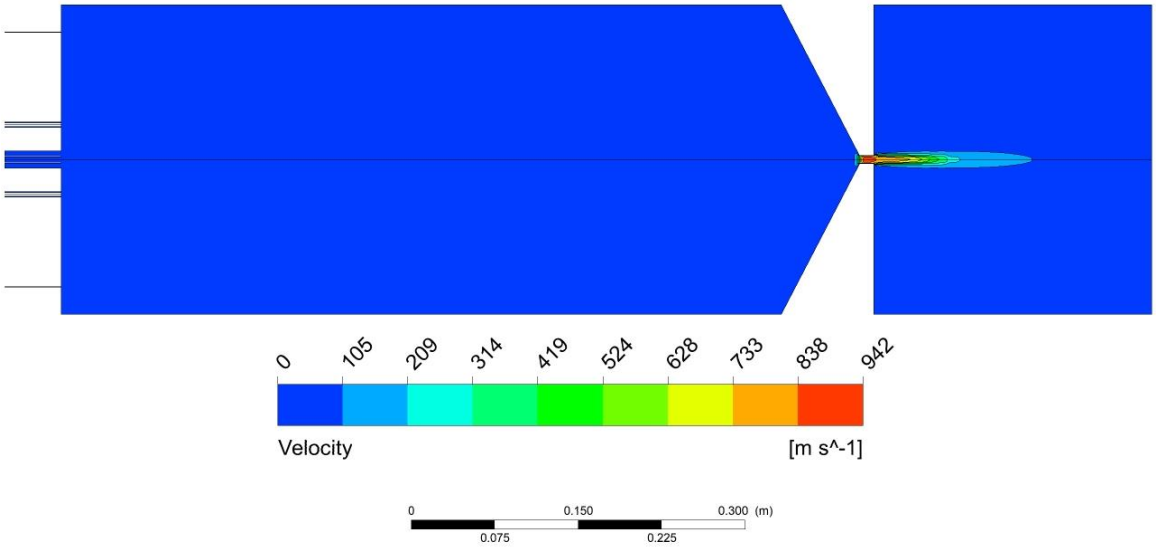

Figure 5.5 – Velocity contours of the HPC.

5.2 – Final Design

The final design assembly of the HPC for operation at 20 bar with 500 kW thermal power input is presented in Figure 5.6. The exploded view of all the components is shown in Figure 5.7. To meet the new requirements, every component of the previous HPC design was modified with the exception of the combustor body. All the modifications will be presented in this section starting from the new front cap to the new end plates.

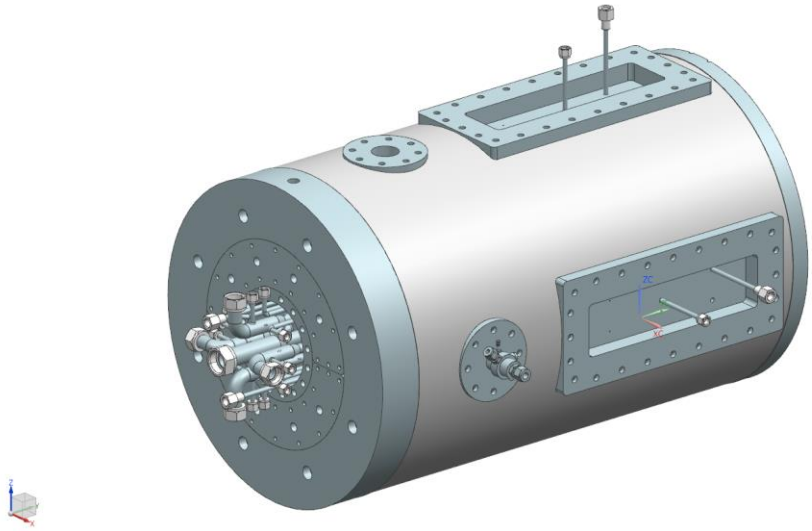

Figure 5.6 – Final assembly of the HPC.

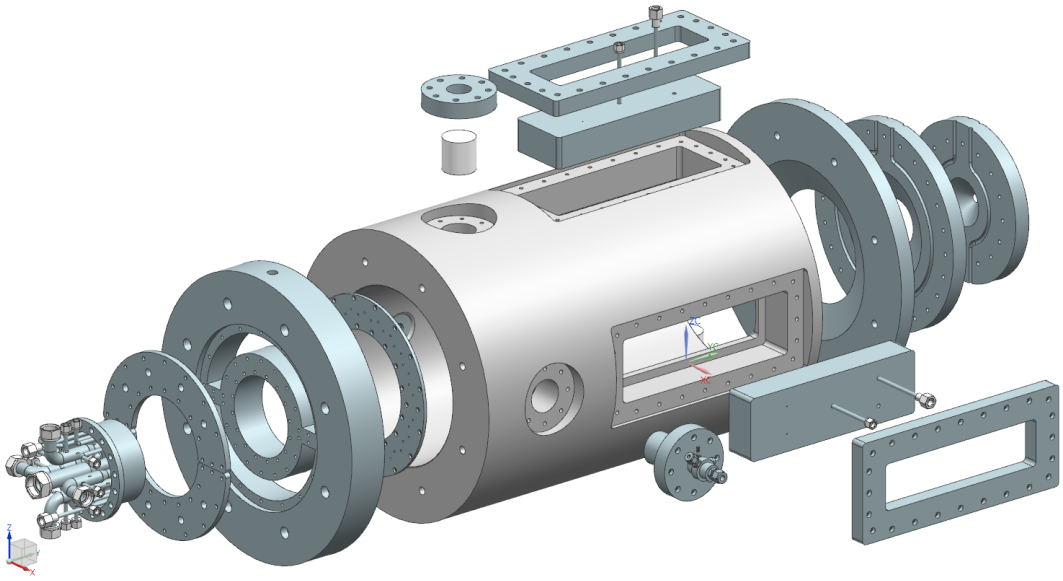

Figure 5.7 – Exploded view of the HPC.

5.2.1 – Front Cap

The front cap was an outer diameter of 18 inches and is made of stainless steel 420. The previous front cap was made of SS 410, but due to material availability and lead time it was decided to manufacture all the new parts with SS 420. SS 420 has very similar thermal and mechanical properties to SS 410 so the change of material didn't have any negative impact. The front cap has an outer diameter of 18 inches to match the combustor body and a thickness of 2.5 in. It is connected to the combustor body using eight ½ - 13 bolts. It has a ¾ - 10 thread located at the top to be lifted with an eyebolt. The new front cap also serves the purpose of housing the 3D printed injector and the CO_2 plates. The hole at the center houses the 3D printed injector and the two half circles at the top and bottom are used to direct the cooling CO_2 stream. The front view and back view can be seen in Fig. 5.8(a) and 5.8(b).

(a) (b)

Figure 5.8 – (a) Front cap face where injector and CO_2 inlet plates attach, (b) Front cap face where CO_2 ring attaches.

5.2.1.1 – Injector

Due to the complicated geometry of the shear co-axial injector, traditional manufacturing would require large cost and lead time. For this reason, it was decided that the injector would be done with additive manufacturing. The injector was printed at UTEP's W.M. Keck center using electron beam melting (EBM) technology. After the part was printed, it was necessary to remove the support material and to perform leak tests. This printing method has a resulting piece with high

porosity with a rough surface finish. Therefore, it was important to perform a leak test to ensure that the tubing and parts were properly sealed. The material used was titanium and it attaches to the front cap using ¼-20 bolts. The injector will be able to withstand the flow rates and pressures associated with the 500 kW and 20 bar requirements. To keep the injector surface that is facing towards the combustion chamber at a low temperature, a flow rate of 9 gpm of water will be fed through the three inlet ports at the top. The injector also has thermocouple ports to measure the temperature 3 mm behind the wall facing the combustion chamber. Three water outlet ports are located at the bottom of the injector. Figures 5.9 (a), (b), and (c) show different views of the 3D printed injector.

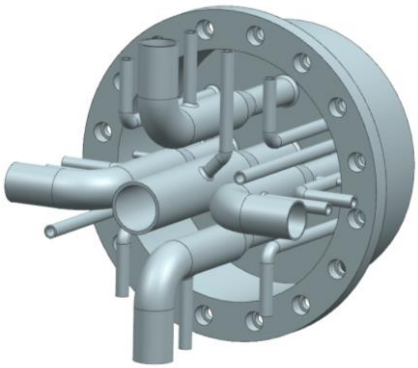

(a)

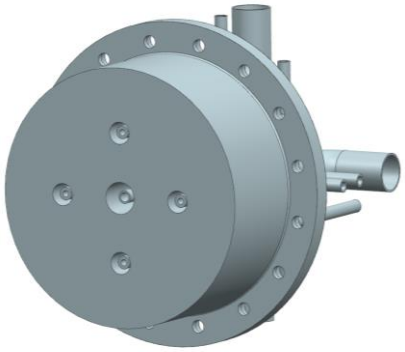

(b)

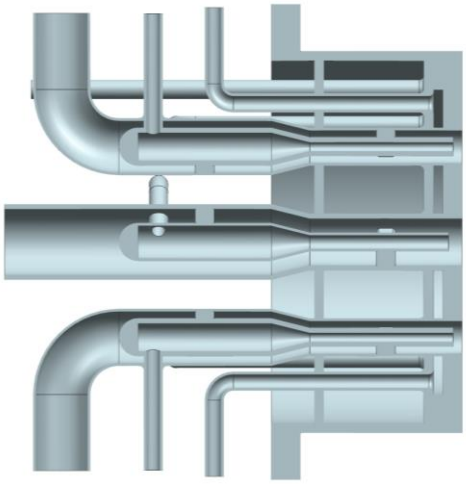

(c)

Figure 5.9 – (a) Inlet section of the injector, (b) outlet section of the injector that faces the combustion chamber, (c) half section cut view of the injector.

5.2.1.2 – CO_2 Cooling Plates

Two different plates of SS 420 were designed to distribute the CO_2. The first plate is a half-circle that is used to seal the chamber into which the CO_2 is fed, Fig. 5.10(a). The front cap has two chambers, so two plates are needed. The reason for having two half-circles is for the front cap to have structural integrity, and base for attachment. To have an evenly distributed gas, the CO_2 is fed through four ½ in diameter evenly spaced ports. These plates have an outside diameter of 11.5 in, an inner diameter of 6.25 in, and a thickness of 0.375 in. They are attached to the front cap using twenty ¼-20 bolts each. The second plate is a full ring that has the purpose of distributing the CO_2 evenly into the combustion chamber in a ring fashion, Fig. 5.10(b). It has forty-two holes with a diameter of 1/8 in evenly distributed along the ring, which gives a total open area of 0.515 in^2. The total open area matches the cross-sectional area of the 1 in feed pipe. The purpose of this is to reduce the pressure drop across the CO_2 distribution system. The second ring plate has an outer diameter of 11.15 in, an inner diameter of 6.85 in, and a thickness of 7/32 in. It is attached to the front cap using thirty-six 10-24 bolts. The simple geometry of this part allows new designs to be implemented. For example, if an increased CO_2 velocity is desired, a new ring with smaller diameter holes or fewer holes can be made.

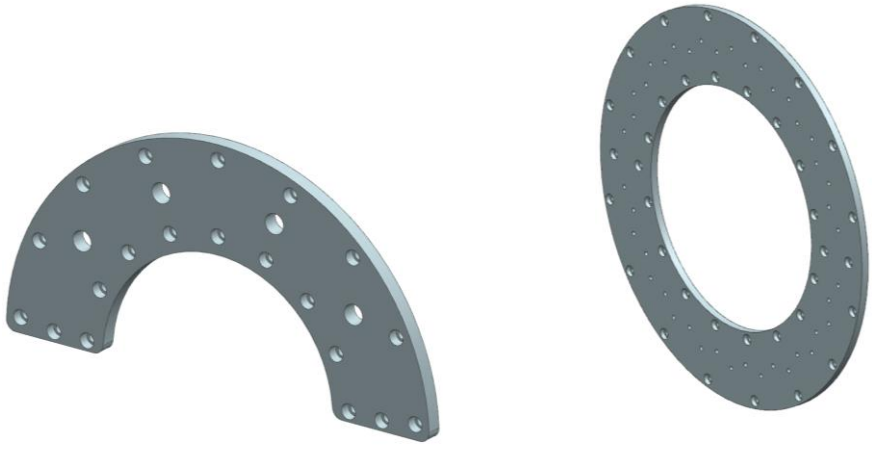

(a) (b)

Figure 5.10 – (a) CO_2 sealing plate (b) CO_2 ring distributor.

5.2.2 – Instrumentation Ports

The instrumentation ports are used as the housing for the ignition source of the system and will also be used as an optical port for flame monitoring. There are a total of 3 instrumentation ports located in the body of the combustor.

5.2.2.1 – Igniters

Two of the ports, located at the left and right of the combustor, will be fitted with the igniters. The igniters will be facing each other and will also use methane and oxygen as the fuel and oxidizer. They are made of stainless steel and are attached to the combustor body using eight ¼-20 bolts.

Figure 5.11 – Igniter front and back view.

5.2.2.2 – Quartz window and window cover

The instrumentation port found at the top of the combustor body will be used as an optically accessible window. The optical access will be used to safely monitor from a remote location if the igniters and injector are working using a camera mounted above the combustor. A clear fused quartz window was manufactured to fit into the hole of the combustor body, Fig. 5.12(a). The quartz window has a diameter of 2.06 in and a length of 2.06 in. The window cover is made of SS 410 and is attached to the combustor body using eight ¼-20 bolts. Its function is to keep the quartz window in place and seal the combustor. The window cover has an outer diameter of 4.5 in, an inner diameter of 1.5 in, and a thickness of 1 in, Fig 5.12(b).

(a) (b)

Figure 5.12 – (a) Fused quartz window, (b) window cover.

5.2.3 – Metal Covers

The metal covers are a replacement for the quartz windows previously used. They are made of SS 420 and have the same general dimensions of the quartz windows of 12.53 x 4.03 x 2.03 in. Due to the new operating pressure of 20 bar, the quartz windows had to be replaced, since they were originally designed to operate at a maximum pressure of 15 bar. The new pressure of 20 bar represents a 28.6% increase. The metal covers are equipped with thermocouples, pressure transducers, and pressure relief valves. The added instrumentation will be used to gather temperature data further down of the combustor and will help us determine when the target pressure is achieved. There are two metal cover designs, the first design, Fig. 5.13(a), has a pressure transducer port at the center and two thermocouple ports. The other two holes are guide holes in case something needs to be fitted later. The second metal cover design, Fig. 5.13(b) has a 1 in NPT hole to fit the pressure relief valve.

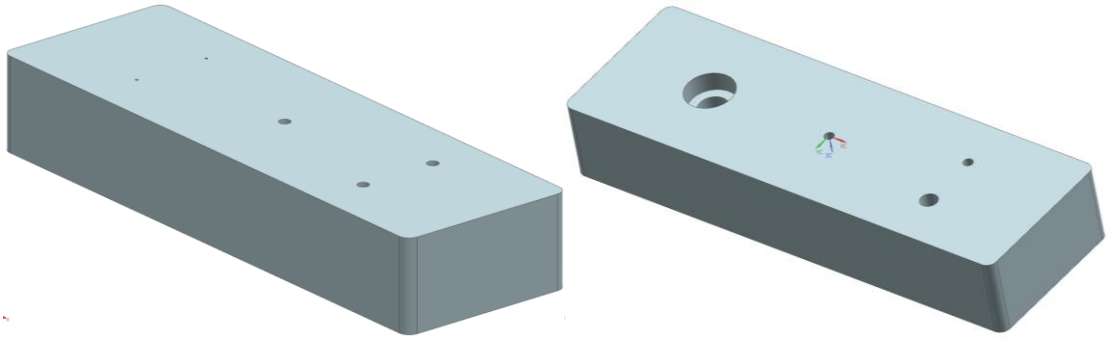

(a) (b)

Figure 5.13 – (a) Metal cover 1, (b) metal cover 2.

5.2.4 – Exit Plates

Three exit plates were designed to have a converging nozzle at an angle of 27.5°. These three plates replace the existing exit cap that isn't angled and doesn't have water cooling. As seen in Figure 5.14, the three plates have channels. These channels will have a copper tube running through it with water running at different flow rates to cool them down. All the plates are made of SS 420 and have a thickness of 1 in. The first plate, Fig. 5.14(a), will attach to the combustor body using eight ¾-10 bolts. It has an outer and inner diameter of 18 in and 7 in. The second plate, Fig. 5.14(b), has an outer and inner diameter of 13 in and 3 in. The second plate uses ¼-20 bolts to attach to the first plate. Finally, the third plate seen in Fig. 5.14(c) has an outer and inner diameter of 10 and 0.4 in. The final diameter will choke the flow and control the combustion chamber pressure of 20 bar. The third plate also used ¼-20 bolts to attach to the second plate.

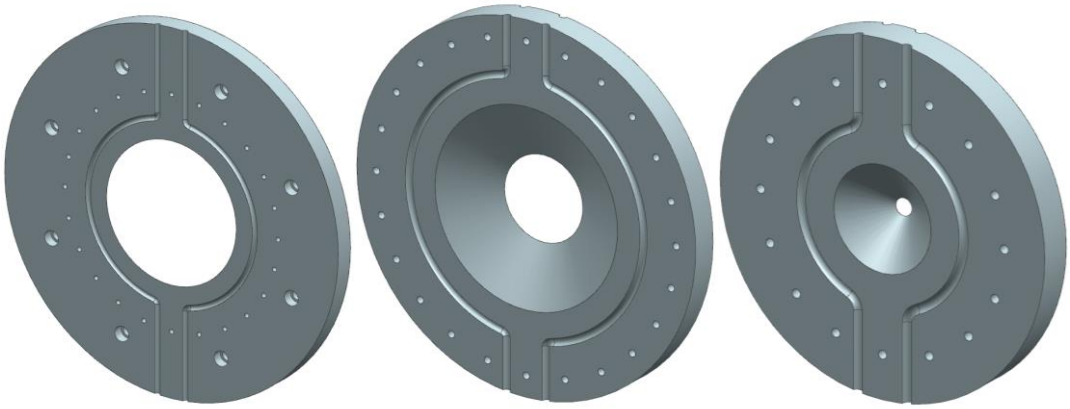

(a) (b) (c)

Figure 5.14 – (a) First exit plate, (b) second exit plate, (c) third exit plate.

5.3 – WATER COOLING

The goal of the cooling circuit design was to flow sufficient water through channels on the injector and on the exit plates to cool them down by transferring the heat to the water and removing it from the parts. The total heat on each part was found from the CFD results. Afterwards, the total heat removal necessary for each componentwas calculated using a 2D thermal resistance model. Finally, the total flow rate of water necessary to remove the heat was calculated. The results are shown in Table 5.1.

Table 5.1 – Water cooling results.

Component	Q removed (kW)	Necessary water flow (gpm)
Injector Face	60	9
End Plate 1	43	7
End Plate 2	17	3
End Plate 3	32	4.8

The injector face needs a higher water flow rate because it is the closest to the combustion flame and because there is a recirculation zone right next to it as shown in the CFD results. The

final end plate needs a high water flow rate because the high velocity gases in that region increase heat transfer.

Based on the calculation, a 3 pump system was proposed to meet the cooling requirements, Fig 5.15. One 10 gpm pump will be used for the injector face, one 10 gpm will be used for end plates 1 and 2, and one 5 gpm pump will be used for end plate 3. To control the water flow, a solenoid valve will be used in each line. A total of six thermocouples will be used, 2 for each line. The thermocouples will be placed before and after entering the heated zone to measure the rise in water temperature and ensure that the cooling system is working as expected. Pressure transducers will be used to monitor the pressure drop in the lines. To remove heavy particles, the feed system will be equiped with a filter. The water cooling system will be an open loop system.

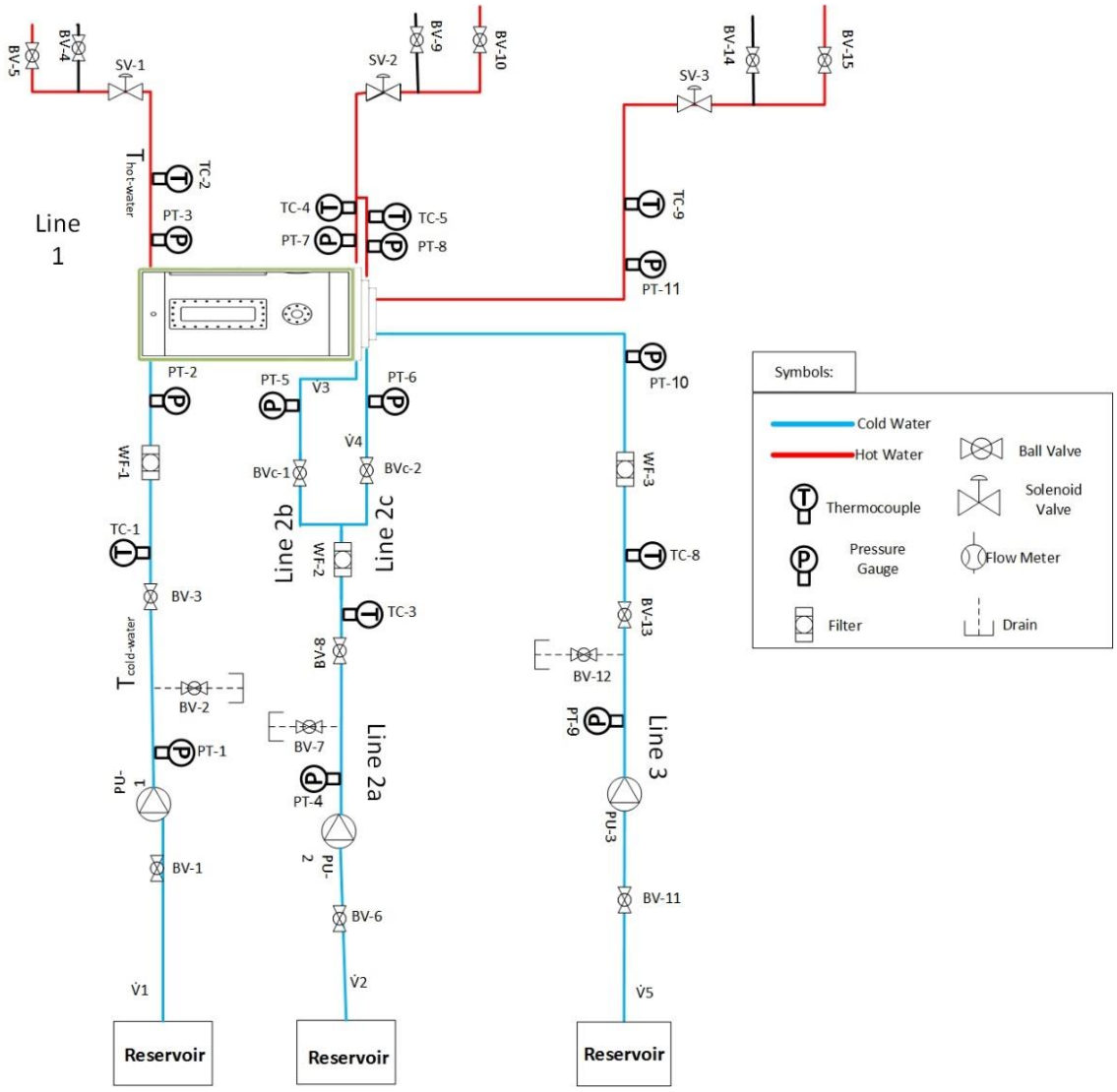

Figure 5.15 – Water feed system schematic.

Chapter 6: Summary and Conclusions

The majority of the greenhouse gas emissions in the US comes from the electricity sector by burning fossil fuels. Environmental regulations have been implemented to reduce the amount of CO_2 emitted into the atmosphere. Despite the grow in renewable sources like solar energy, forecasts show that natural gas will be the main source of electricity in the near-term future. One method to reduce the greenhouse gas emissions to the atmosphere is oxy-fuel technology. The main objective of this thesis was to design and develop a steady-state high pressure combustor that uses oxygen and methane with a thermal power input of 500 kW and operation at 20 bar pressure.

The following steps were conducted to design and develop the combustor. The necessary flow rates of methane and oxygen were determined for 500 kW of power input at stoichiometric conditions. These mass flow rates are 0.01 kg/s for CH_4 and 0.04 kg/s for O_2. The injector parameters for effective mixing, such as momentum flux ratio, was determined. It was found that a momentum flux ratio of 12 would ensure proper mixing of the fuel and oxidizer gases. The injector design for 3D printing was proposed utilizing EBM technology. The adiabatic flame temperature of oxy-methane combustion was calculated and found to be 3500 K at stoichiometric conditions. The inner wall temperature of the combustion chamber without any cooling was calculated and was found to be above material limits. A structural analysis was done to determine the thermal and mechanical stress and to set the maximum allowable inner wall temperature. The maximum allowable inner wall temperature was determined to be 600 K. The throat diameter necessary to keep the combustion chamber at a pressure of 20 bar was calculated to be 10.4 mm. A numerical analysis was done to determine the effect of room temperature CO_2 injected along the inner walls on wall temperature.

It was found through the CFD analysis that gas recirculation zones were keeping the inner walls of the combustor above the allowable temperature. Modifying the exit cap from a straight end to a 27.5° resulted in favorable results to diminish the recirculation zones and keeping the walls below the material limits. It was also found through the CFD analysis that the injection of

0.09 kg/s of CO_2 at 10 m/s would effectively shield and maintain an allowable temperature of 600 K at the inner walls of the combustor, but only for ¾ of the total length of the combustion chamber. To cool down the injector face and the end plates, an active water cooling solution with mass flowrates of up to 9 gpm was proposed.

Finally, the previous HPC design was assessed and the necessary modifications to meet the new project requirements were proposed. The proposed modification designs are presented and include their description and purpose.

References

[1] O. US EPA, "Sources of Greenhouse Gas Emissions," *epa.gov*, 2017. [Online]. Available: https://www.epa.gov/ghgemissions/sources-greenhouse-gas-emissions. [Accessed: 02-Jun-2017].

[2] U. S. D. of Energy, "Electricity in the United States - Energy Explained, Your Guide To Understanding Energy - Energy Information Administration," *eia.gov*, 2017. [Online]. Available: https://www.eia.gov/energyexplained/index.cfm?page=electricity_in_the_united_states. [Accessed: 04-Jun-2017].

[3] U. S. D. of Energy, "Use of Natural Gas - Energy Explained, Your Guide To Understanding Energy - Energy Information Administration," *eia.gov*, 2016. [Online]. Available: https://www.eia.gov/energyexplained/index.cfm?page=natural_gas_use. [Accessed: 04-Jun-2017].

[4] American Electric Power, "AEP.com - Natural Gas," 2017. [Online]. Available: https://www.aep.com/about/IssuesAndPositions/Generation/Technologies/NaturalGas.aspx. [Accessed: 04-Jun-2017].

[5] U.S. Energy Information Administration, "Short-Term Energy Outlook - U.S. Energy Information Administration (EIA)," 2017. [Online]. Available: https://www.eia.gov/outlooks/steo/report/renew_co2.cfm. [Accessed: 04-Jun-2017].

[6] U.S. Energy Information Administration, *International Energy Outlook 2016*, vol. 0484(2016), no. May 2016. 2016.

[7] Y. Mulugetta, E. Hertwich, K. Riahi, T. Gibon, and K. Neuhoff, "Climate Change 2014: Mitigation of climate change," *IPCC Fifth Assess. Rep.*, pp. 527–532, 2014.

[8] T. Fout *et al.*, "Cost and Performance Baseline for Fossil Energy Plants Volume 1a: Bituminous Coal (PC) and Natural Gas to Electricity Revision 3," *Natl. Energy Technol. Lab.*, vol. 1a, no. May, p. 240, 2015.

[9] CCS Network, "What & How of CCS - CCS101 - What & How of CCS," 2017. [Online]. Available: http://ccs101.ca/ccs_pro/what__how_of_ccs. [Accessed: 14-Jun-2017].

[10] CCS Network, "Post-Combustion - CCS101 - Post-Combustion," 2017. [Online]. Available: http://ccs101.ca/ccs_pro/what__how_of_ccs/co2_capture_methods/postcombustion. [Accessed: 14-Jun-2017].

[11] The Linde Group, "Post-combustion | The Linde Group," 2017. [Online]. Available: http://www.the-linde-group.com/en/clean_technology/clean_technology_portfolio/carbon_capture_storage/postcombustion_pilot_plants/index.html. [Accessed: 14-Jun-2017].

[12] P. L. Spath and M. K. Mann, "Life Cycle Assessment of a Natural Gas Combined Cycle Power Generation System," pp. 1–56, 2000.

[13] National Energy Technology Laboratory, "Oxy-Combustion | netl.doe.gov," 2017. [Online]. Available: https://www.netl.doe.gov/research/coal/energy-systems/advanced-combustion/oxy-combustion. [Accessed: 17-Jun-2017].

[14] J. D. Figueroa, T. Fout, S. Plasynski, H. McIlvried, and R. D. Srivastava, "Advances in CO2 capture technology-The U.S. Department of Energy's Carbon Sequestration Program," *Int. J. Greenh. Gas Control*, vol. 2, no. 1, pp. 9–20, 2008.

[15] J. Xiong, H. Zhao, and C. Zheng, “Thermoeconomic cost analysis of a 600MW e oxy-combustion pulverized-coal-fired power plant,” *Int. J. Greenh. Gas Control*, vol. 9, pp. 469–483, 2012.
[16] J. Davison, “Performance and costs of power plants with capture and storage of CO2,” *Energy*, vol. 32, no. 7, pp. 1163–1176, 2007.
[17] C. D. Slabaugh *et al.*, “The development of an optically accessible, high-power combustion test rig,” *Rev. Sci. Instrum.*, vol. 85, no. 3, 2014.
[18] National Energy Technology Laboratory, “hp combustion facility | netl.doe.gov.” [Online]. Available: https://www.netl.doe.gov/research/on-site-research/research-capabilities/hp-combustion-facility. [Accessed: 29-Jun-2017].
[19] S. Gadiraju, S. V Ekkad, H. Moon, Y. Kim, and R. Srinivasan, “Gt2016-57825 Gas Turbine Combustor Rig Development and Initial Observations,” pp. 1–12, 2016.
[20] S. Daniele, P. Jansohn, J. Mantzaras, and K. Boulouchos, “Turbulent flame speed for syngas at gas turbine relevant conditions,” *Proc. Combust. Inst.*, vol. 33, no. 2, pp. 2937–2944, 2011.
[21] University of California Irvine Combustion Laboratory, “UCICL: COMBUSTION SCIENCE RESOURCES | Test Cells,” 2010. [Online]. Available: http://www.ucicl.uci.edu/2/RESEARCHPROJECTS/CombustionScienceResources/TestCells/Index.aspx. [Accessed: 05-Jul-2017].
[22] X. Qin and Y. Ju, “Measurements of burning velocities of dimethyl ether and air premixed flames at elevated pressures,” *Proc. Combust. Inst.*, vol. 30, no. 1, pp. 233–240, 2005.
[23] M. P. Burke, X. Qin, Y. Ju, and F. L. Dryer, “Measurements of Hydrogen Syngas Flame Speeds at Elevated Pressures,” pp. 1–14, 2007.
[24] C. A. VALDEZ, “DEVELOPMENT OF THE CONTROL AND IGNITION SYSTEMS ON A HIGH PRESSURE GAS TURBINE COMBUSTOR,” The University of Texas at El Paso, 2012.
[25] J. N. MICHEL, “Design and development of an optically accessible high pressure combustor,” The University of Texas at El Paso, 2012.
[26] D. R. Noble, Q. Zhang, A. Shareef, J. Tootle, A. Meyers, and T. Lieuwen, “Syngas Mixture Composition Effects Upon Flashback and Blowout,” in *Volume 1: Combustion and Fuels, Education*, 2006, vol. 2006, pp. 357–368.
[27] Pennsylvania State University, “Facilities - Combustion Testing,” 2016. [Online]. Available: http://www.hpcl.psu.edu/Facilities - Combustion Testing.html. [Accessed: 24-Jul-2017].
[28] J. S. Santner *et al.*, “Combustion at High Pressure,” p. 6.
[29] S. E. M. JURADO, “EXPERIMENTAL INVESTIGATION OF SYNGAS FLAME STABILITY USING A MULTI-TUBE FUEL INJECTOR IN A HIGH PRESSURE COMBUSTOR,” The University of Texas at El Paso, 2014.
[30] S. Hossain, “EXPERIMENTAL EVALUATION OF FLAME STABILITY AND POLLUTANT EMISSIONS FROM A MULTI-TUBE FUEL INJECTOR,” The University of Texas at El Paso, 2014.
[31] S. R. Turns, *An Introduction to Combustion: Concepts and Applications*, 2nd ed. McGraw-Hill, 2000.
[32] A. S. M. A. Chowdhury, J. Cruz, J. Aboud, A. Rios, A. Choudhuri, and N. D. Love, “Design and Experimental Demonastration of a High Pressure Oxy-Methane Combustor,” *Am. Inst. Aeronaut. Astronaut.*, pp. 1–8, 2017.

[33] J. Lux and O. Haidn, “Effect of Recess in High-Pressure Liquid Oxygen/Methane Coaxial Injection and Combustion,” *J. Propuls. Power*, vol. 25, no. 1, pp. 24–32, Jan. 2009.
[34] D. Kendrick, G. Herding, P. Scouflaire, C. Rolon, and S. Candel, “Effects of a recess on cryogenic flame stabilization,” *Combust. Flame*, vol. 118, no. 3, pp. 327–339, 1999.
[35] A. Tripathi, M. Juniper, P. Scouflaire, J.-C. Rolon, D. Durox, and S. Candel, “LOx tube recess in cryogenic flames investigated using OH and H2O emission,” in *35th Joint Propulsion Conference and Exhibit*, 1999.
[36] D. B. Wheeler and F. M. Kirby, “High-Pressure LOX/CH4 Injector Program,” *Nasa-Cr-161342*, 1979.
[37] National Aeronautics and Space Administration, “CEARUN,” 2016. [Online]. Available: https://cearun.grc.nasa.gov/. [Accessed: 16-Jul-2017].
[38] A. G. Y.A. Cengel, *Heat and Mass Transfer: Fundamentals and Applications*, 4th ed. McGraw-Hill, 2010.
[39] A. Rios, J. Cruz, A. A. Chowdhury, A. Choudhuri, and N. Love, “FINITE ELEMENT ANALYSIS OF COMBUSTOR EXPOSED TO A HIGH TEMPERATURE HIGH-PRESSURE ENVIRONMENT,” in *The Southwest Emerging Technology Symposium*, 2017, pp. 2–8.
[40] D. H. Huang and D. K. Huzel, *Modern Engineering for Design of Liquid-Propellant Rocket Engines*. Washington DC: American Institute of Aeronautics and Astronautics, 1992.
[41] American Iron and Steel Institute, “High-Temperature Characteristics of Stainless Steels.” Nickel Development Institute, pp. 1–47.
[42] L. E. Sanchez, J. Chaparro, S. A. Torres, N. D. Love, and A. R. Choudhuri, “Development and Testing of a O_2/CH_4 Torch Igniter for Propulsion Systems,” *52nd AIAA/SAE/ASEE Jt. Propuls. Conf.*, pp. 1–8, 2016.
[43] I. SAS IP, “Fluent Theory Guide,” 2017. [Online]. Available: https://www.sharcnet.ca/Software/Ansys/16.2.3/en-us/help/flu_th/flu_th.html. [Accessed: 25-Jul-2017].

Appendix

- NASA CEA code used for oxy-methane combustion at 20 bar and equivalence ratio of 1. Solver used was for constant pressure.

Input:

```
      NASA-GLENN CHEMICAL EQUILIBRIUM PROGRAM CEA2, FEBRUARY 5, 2004
                  BY  BONNIE MCBRIDE AND SANFORD GORDON
       REFS: NASA RP-1311, PART I, 1994 AND NASA RP-1311, PART II, 1996

*******************************************************************************

prob case=asda7008  hp p(bar)=20
phi=1
reac
 fuel  CH4             wt%= 100.0 t,k= 298.15
 oxid  O2              wt%= 100.0 t,k=  298.15
  output massf
output trans
output short
output trace= 1e-5
end
```

Output:

```
        THERMODYNAMIC EQUILIBRIUM COMBUSTION PROPERTIES AT ASSIGNED

                              PRESSURES

CASE = asda7008

            REACTANT                    WT FRACTION      ENERGY      TEMP
                                         (SEE NOTE)     KJ/KG-MOL      K
FUEL        CH4                           1.0000000    -74600.000    298.150
OXIDANT     O2                            1.0000000         0.000    298.150

O/F=    3.98926  %FUEL= 20.043038  R,EQ.RATIO= 1.000000  PHI,EQ.RATIO= 1.000000

THERMODYNAMIC PROPERTIES

P, BAR             20.000
T, K             3447.70
RHO, KG/CU M    1.5577 0
H, KJ/KG          -932.03
U, KJ/KG         -2215.99
G, KJ/KG         -43155.4
S, KJ/(KG)(K)     12.2468

M, (1/n)           22.326
(dLV/dLP)t       -1.05421
(dLV/dLT)p         1.9906
Cp, KJ/(KG)(K)     9.0031
GAMMAs             1.1232
SON VEL,M/SEC      1200.9

TRANSPORT PROPERTIES (GASES ONLY)
  CONDUCTIVITY IN UNITS OF MILLIWATTS/(CM)(K)

VISC,MILLIPOISE    1.1169

 WITH EQUILIBRIUM REACTIONS

Cp, KJ/(KG)(K)     9.0031
CONDUCTIVITY      20.1773
PRANDTL NUMBER     0.4984

 WITH FROZEN REACTIONS

Cp, KJ/(KG)(K)     2.2007
CONDUCTIVITY       3.6178
PRANDTL NUMBER     0.6794

MASS FRACTIONS

*CO              1.8554-1
*CO2             2.5830-1
COOH             1.1474-5
*H               1.2935-3
HO2              2.5935-4
*H2              5.3914-3
H2O              3.5007-1
H2O2             2.5110-5
*O               1.8643-2
*OH              7.6001-2
*O2              1.0445-1

 * THERMODYNAMIC PROPERTIES FITTED TO 20000.K

NOTE. WEIGHT FRACTION OF FUEL IN TOTAL FUELS AND OF OXIDANT IN TOTAL OXIDANTS
```

CEA code with CO_2 dilution

NASA CEA code used for oxy-methane combustion at 20 bar and equivalence ratio of 1 with 50% dilution of CO_2 by volume. Solver used was for rockets although using the constant pressure solver yields the same result for properties in the combustion chamber. This solver was used to find properties at the throat such as the sonic velocity. The CO_2 was input in the oxidizer stream. The throat and exit values are identical because there is no expansion zone like in a rocket. In other words, the throat is the exit. After calculating the mass flow of CO_2 corresponding to 50% CO_2 by volume, the weight percent of oxygen and CO_2 were calculated using the following formulas and input to the code in lines 19 and 20. The code can be adjusted by inputting different wt% values depending on the desired dilution of CO_2 in the mix.

$$wt\%\ of\ CO_2 = \frac{\dot{m}CO_2}{\dot{m}CO_2 + \dot{m}O_2}$$

$$wt\%\ of\ O_2 = \frac{\dot{m}O_2}{\dot{m}CO_2 + \dot{m}O_2}$$

Input:

```
1
2
3          NASA-GLENN CHEMICAL EQUILIBRIUM PROGRAM CEA2, FEBRUARY 5, 2004
4                    BY  BONNIE MCBRIDE AND SANFORD GORDON
5        REFS: NASA RP-1311, PART I, 1994 AND NASA RP-1311, PART II, 1996
6
7   ****************************************************************************
8
9
10  prob case=ghsd6131 ro equilibrium
11
12
13   ! iac problem
14  phi 1
15  p,bar  20
16  supar 1
17  reac
18   fuel  CH4 wt%=100 t,k=298.15
19   oxid O2 wt%=30.629 t,k=298.15
20   oxid CO2 wt%=69.371 t,k=298.15
21  output trans
22  output    short
23  output trace=1e-5
24  end
```

Output:

```
          THEORETICAL ROCKET PERFORMANCE ASSUMING EQUILIBRIUM

        COMPOSITION DURING EXPANSION FROM INFINITE AREA COMBUSTOR

Pin =   290.1 PSIA
CASE = ghsd6131

          REACTANT                    WT FRACTION      ENERGY      TEMP
                                       (SEE NOTE)     KJ/KG-MOL      K
FUEL      CH4                         1.0000000    -74600.000    298.150
OXIDANT   O2                          0.3062900         0.000    298.150
OXIDANT   CO2                         0.6937100   -393510.000    298.150

O/F=   13.02447  %FUEL=  7.130397  R,EQ.RATIO= 1.000000  PHI,EQ.RATIO= 1.000000

                CHAMBER   THROAT     EXIT
Pinf/P            1.0000   1.7268   1.7268
P, BAR           20.000   11.582   11.582
T, K           2498.05  2365.53  2365.53
RHO, KG/CU M  3.3647 0 2.0702 0 2.0702 0
H, KJ/KG      -6092.08 -6407.18 -6407.18
U, KJ/KG      -6686.49 -6966.64 -6966.64
G, KJ/KG      -26648.7 -25873.3 -25873.3
S, KJ/(KG)(K)    8.2291   8.2291   8.2291

M, (1/n)         34.942   35.156   35.156
(dLV/dLP)t    -1.00748 -1.00552 -1.00552
(dLV/dLT)p       1.1989   1.1552   1.1552
Cp, KJ/(KG)(K)   2.9158   2.6798   2.6798
GAMMAs           1.1234   1.1265   1.1265
SON VEL,M/SEC     817.2    793.9    793.9
MACH NUMBER       0.000    1.000    1.000

TRANSPORT PROPERTIES (GASES ONLY)
  CONDUCTIVITY IN UNITS OF MILLIWATTS/(CM)(K)

VISC,MILLIPOISE  0.88131  0.84932  0.84932

 WITH EQUILIBRIUM REACTIONS

Cp, KJ/(KG)(K)   2.9158   2.6798   2.6798
CONDUCTIVITY     3.9761   3.4855   3.4855
PRANDTL NUMBER   0.6463   0.6530   0.6530

 WITH FROZEN REACTIONS

Cp, KJ/(KG)(K)   1.6536   1.6444   1.6444
CONDUCTIVITY     2.1111   2.0151   2.0151
PRANDTL NUMBER   0.6903   0.6931   0.6931

PERFORMANCE PARAMETERS

Ae/At                     1.0000   1.0000
CSTAR, M/SEC              1216.9   1216.9
CF                        0.6523   0.6523
Ivac, M/SEC               1498.6   1498.6
Isp, M/SEC                 793.9    793.9

MOLE FRACTIONS

*CO            3.7739-2 2.7874-2 2.7874-2
*CO2           6.2908-1 6.4302-1 6.4302-1
*H             3.0306-4 1.9000-4 1.9000-4
*H2            2.9463-3 2.2982-3 2.2982-3
H2O            3.0395-1 3.0764-1 3.0764-1
*O             4.3521-4 2.4790-4 2.4790-4
*OH            7.1199-3 4.9549-3 4.9549-3
*O2            1.8414-2 1.3767-2 1.3767-2

 * THERMODYNAMIC PROPERTIES FITTED TO 20000.K

NOTE. WEIGHT FRACTION OF FUEL IN TOTAL FUELS AND OF OXIDANT IN TOTAL OXIDANTS
```

Wall temperature calculation for oxy-methane combustion, no CO_2 dilution.

The gas properties were taken from the code without CO_2 dilution and input into the following equations.

To calculate the Reynolds number, the following formulas are used:

$$Re = \frac{\rho V D}{\mu}$$

Knowing that,

$$V = \frac{\dot{m}}{\rho A}$$

And,

$$A = \frac{\pi}{4} D^2$$

And substituting both into the first formula yields:

$$Re = \frac{4\dot{m}}{\mu \pi D}$$

The values used are a total mass flow rate of $\dot{m} = 0.05$ kg/s, a viscosity of μ =1.1169E-4 kg/m-s, and a hydraulic diameter of D = 0.2794 m (11 in). Which yields a Reynold's number of Re = 2040. Afterwards the Nusselt number was calculated with the following formula:

$$Nu = \frac{\left(f/8\right) Re\ Pr}{1.07 + 12.7\left(f/8\right)^{0.5}\left(Pr^{2/3} - 1\right)}$$

Where,

$$f = (0.79\ln(Re) - 1.64)^{-2}$$

The values used are Re=2040, Prandtl number of Pr = 0.4984, and friction factor of f = 0.0521. The Nusselt number is then found to be Nu = 9.607.

Finally, the convective heat transfer coefficient can be found from:

$$h = \frac{Nu\ k}{D}$$

Where Nu=9.607, the thermal conductivity of the gas is k = 2.017 W/m-K, and D = 0.2794 m. The convective heat transfer coefficient is found to be h = 69.35 W/m^2-K.

Knowing the convective heat transfer coefficient of the hot gas side, it is possible to calculate the inner and outer wall temperatures if steady state is assumed. A simple 2D heat resistance model is used.

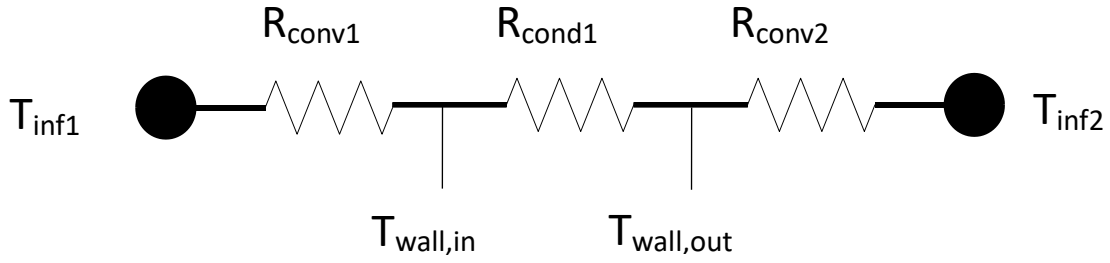

Where:

- T_{infl} = Adiabatic flame temperature = 3447.7 K
- T_{inf2} = Environment temperature = 298 K
- $A_1 = Inner\ surface\ area = \pi D_i L = \pi$*0.2794 m*0.6477 m = 0.568 m
- $A_2 = Outer\ surface\ area = \pi D_o L = \pi$*0.4572m*0.6477m = 0.930 m
- $L = Combustor\ length = 0.6477\ m$
- $k = Thermal\ conductivity\ of\ SS410\ @\ 760\ °C = 30.8 \frac{W}{m-k}$

Knowing this, it is possible to calculate the total thermal resistance by:

- $R_{conv1} = Convective\ resistance\ from\ hot\ gases = \frac{1}{h1*A1} = \frac{1}{69.35\frac{W}{m^2-K}*0.568m} = 0.025 \frac{K}{W}$
- $R_{cond1} = Conductive\ resistance\ along\ wall\ thickness = \frac{ln(r2/r1)}{2\pi kL} = \frac{ln(.2286m/.1397m)}{2*\pi*30.8\frac{W}{m-K}*.6477m} = .004 \frac{K}{W}$
- $R_{conv2} = Convective\ resistance\ from\ environment\ gas = \frac{1}{h2*A2} = \frac{1}{5\frac{W}{m^2-K}*0.930m} = 0.21 \frac{K}{W}$
- $R_{Total} = 0.244 \frac{K}{W}$

The heat loss can then be calculated by:

- $\dot{Q} = \frac{T_{inf1}-T_{inf2}}{R_{Total}} = \frac{3447.7K-298K}{0.244\frac{K}{W}} = 12894\ W$

And the inner wall temperature can be calculated by:

- $\dot{Q} = \frac{T_{inf1}-T_{wall,in}}{R_{conv1}} \rightarrow 12894\ W = \frac{3447.7\ K-T_{wall,in}}{0.03\frac{K}{W}} \rightarrow T_{wall,in} = 3120\ K$

Wall temperature calculation for oxy-methane combustion, no CO_2 dilution.

The following steps were used to calculate the volumetric and mass flow rates of CO_2. To calculate the volumetric flow rate, it was first necessary to know the total volume flow rate of methane and oxygen. Since we know from the input power and stoichiometric conditions that the mass flow rate of oxygen and methane are 0.04 kg/s and 0.01 kg/s respectively, it was possible to calculate the volumetric flow rate using the density of those gases at 20 bar and 25 ºC. The following calculation example is for 50% CO_2 by volume.

$$\dot{V}_{CH_4} = \frac{\dot{m}_{CH_4}}{\rho_{CH_4}} = \frac{0.01\,{}^{kg}/_{s}}{13.4\,{}^{kg}/_{m^3}} = 7.46E-4\,\frac{m^3}{s}$$

$$\dot{V}_{O_2} = \frac{\dot{m}_{O_2}}{\rho_{O_2}} = \frac{0.04\,{}^{kg}/_{s}}{26.14\,{}^{kg}/_{m^3}} = 15.3E-4\,\frac{m^3}{s}$$

$$\dot{V}_{CO_2} = \left[\frac{\left(\dot{V}_{CH_4} + \dot{V}_{O_2}\right)(Desired\ \%)}{100 - Desired\ \%}\right] = \left[\frac{\left(7.46E-4\,\frac{m^3}{s} + 15.3E-4\,\frac{m^3}{s}\right)(50)}{100-50}\right]$$

$$= 22.76E-4\,\frac{m^3}{s}$$

After calculating the volumetric flow rate, the mass flow rate can be calculated by using the density of CO_2 at 20 bar and 25 ºC.

$$\dot{m}_{CO_2} = \dot{V}_{CO_2}\rho_{CO_2} = \left(22.76-4\,\frac{m^3}{s}\right)\left(39.8\,{}^{kg}/_{m^3}\right) = 0.09\,{}^{kg}/_{s}$$

Throat diameter calculation

To calculate the throat diameter, the critical pressure was calculated first using the following formula and values obtained from the NASA CEA results with 50% CO_2 dilution.

$$P_c = P_1\left(\frac{2}{k+1}\right)^{\frac{k}{k-1}} = 20\ bar\left(\frac{2}{1.12+1}\right)^{\frac{1.12}{1.12-1}} = 11.6\ bar$$

This means that the flow will be choked unless the pressure downstream is 11.6 bar or higher. Since the combustor discharges into the atmosphere (1 bar) it is concluded that the flow at the exit will be sonic. Knowing that the exit velocity will be sonic means that the Mach number will be equal to 1. This allows for the use of a simplified equation to calculate the necessary throat area at the exit.

$$A_{throat} = \frac{\dot{m}_{total}}{\sqrt{k\rho P_1\left(\frac{2}{k+1}\right)^{\frac{k+1}{k-1}}}} = \frac{0.14\ kg/s}{\sqrt{1.12 * 3.3647\ {}^{kg}/_{m^3} * 2E6\ Pa * \left(\frac{2}{1.12+1}\right)^{\frac{1.12+1}{1.12-1}}}}$$

$$A_{throat} = 8.5E-5\ m^2$$

Afterwards, the throat diameter can be calculated from:

$$D_{throat} = \sqrt{\frac{4 * A_{throat}}{\pi}} = \sqrt{\frac{4 * 8.5E-5m^2}{\pi}} = 0.0104\ m = 10.4\ mm$$

2D Geometry adaptation

To adapt a 3D geometry into a 2D model the first step is to know the distance from the center of the combustor to the center of the port. For example, the CO_2 distributor plate has all the holes at 0.1143 m from the center. Calculating the total area of the holes yields 4.25 E-4 m^2.

The centerline (C) of a ring is the average of the outer and inner radiuses given by:

$$C = \frac{R_o + R_i}{2}$$

Using the value of C=0.1143 and solving for the outer radius R_o.

$$R_o = 0.2286 - R_i$$

And squaring the answer yields,

$$R_o^2 = R_i^2 - 0.4572R_i + 0.05225$$

The area of the ring that will be formed must be equal to the total area of the holes. The area of a ring is given by:

$$A_{holes} = A_{ring} = \pi(R_o^2 - R_i^2)$$

Subsisting R_o^2 into the previous equation and solving for R_i yields:

$$R_i = \left(0.05225 - \frac{A_{holes}}{\pi}\right)\left(\frac{1}{0.4572}\right)$$

$$R_i = \left(0.05225 - \frac{4.25E-4}{\pi}\right)\left(\frac{1}{0.4572}\right)$$

$$R_i = 0.114004\, m = 114.004\, mm$$

Finally,

$$R_o = 0.2286 - 0.1140004 = 0.114596\, m = 114.596\, mm$$

Therefore, to create a ring representation for a 2D model of all the open area holes in the CO_2 ring distributor, an outer and inner radius of 114.6 mm and 114 mm respectively have to be created. The result can be checked by calculating the area of the ring and matching it to the total area of the holes.

Material Properties

All material properties are taken from [41].

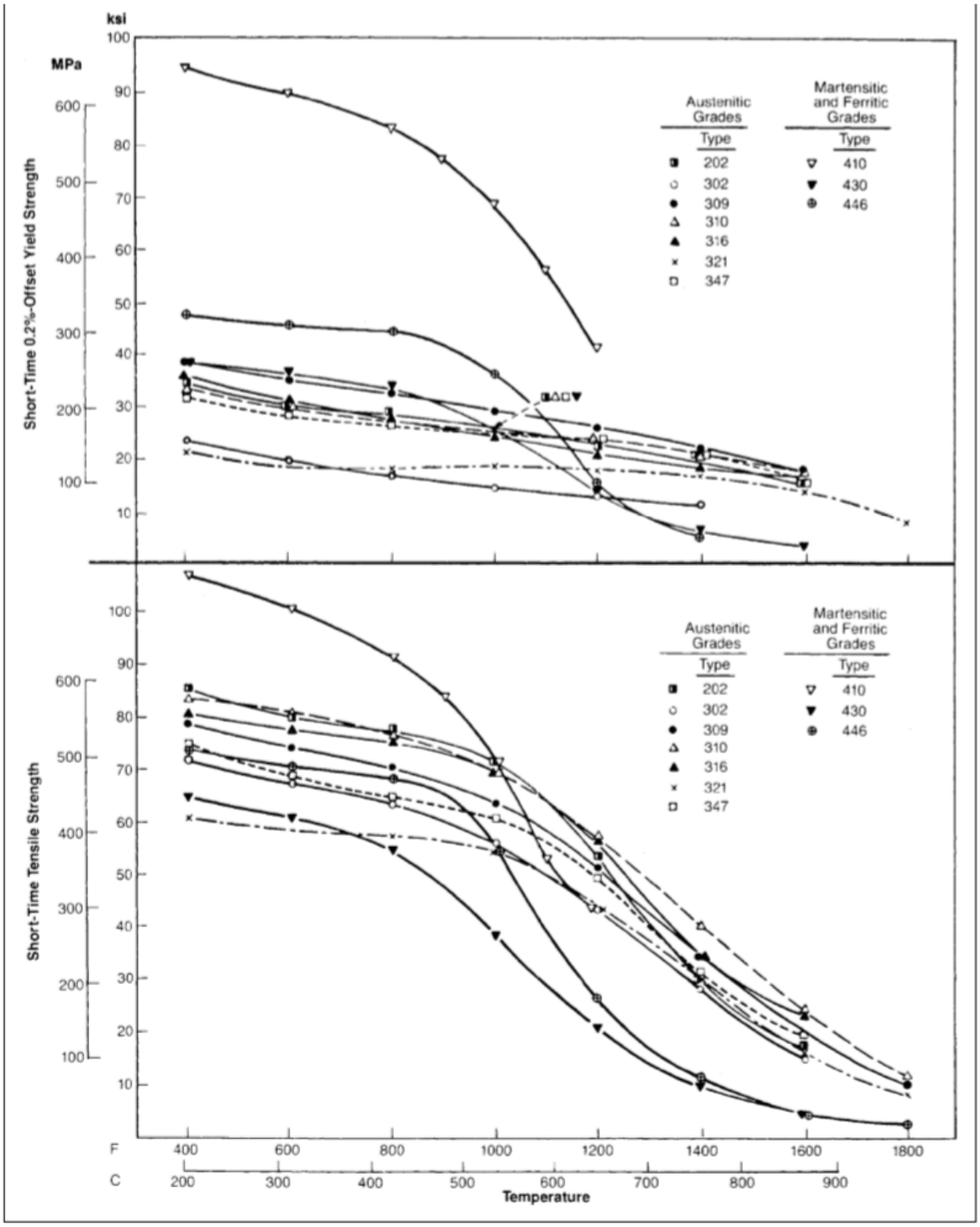

Linear Thermal Expansion of the Three Main Classes of Stainless Steel (1)

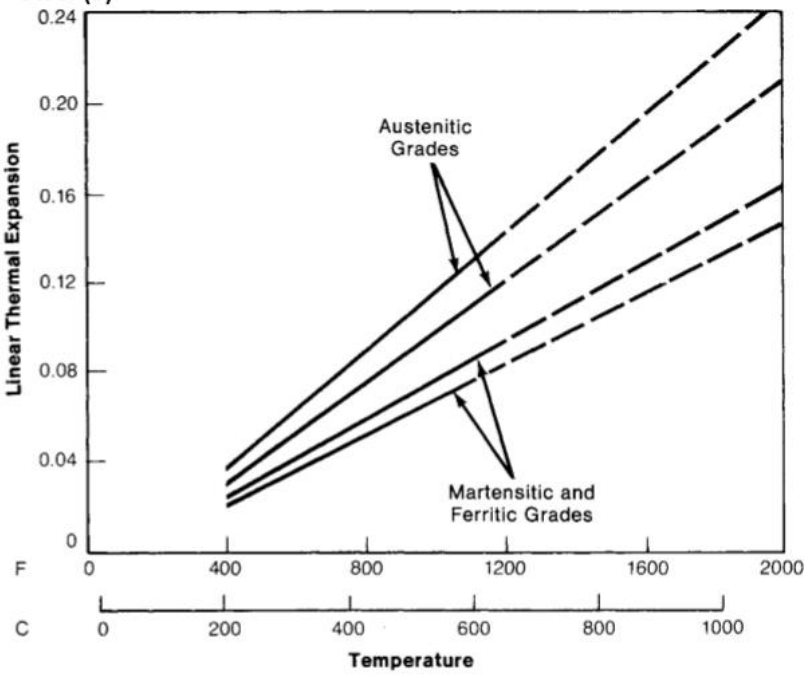

Thermal Conductivity of the Three Main Classes of Stainless Steel (1)

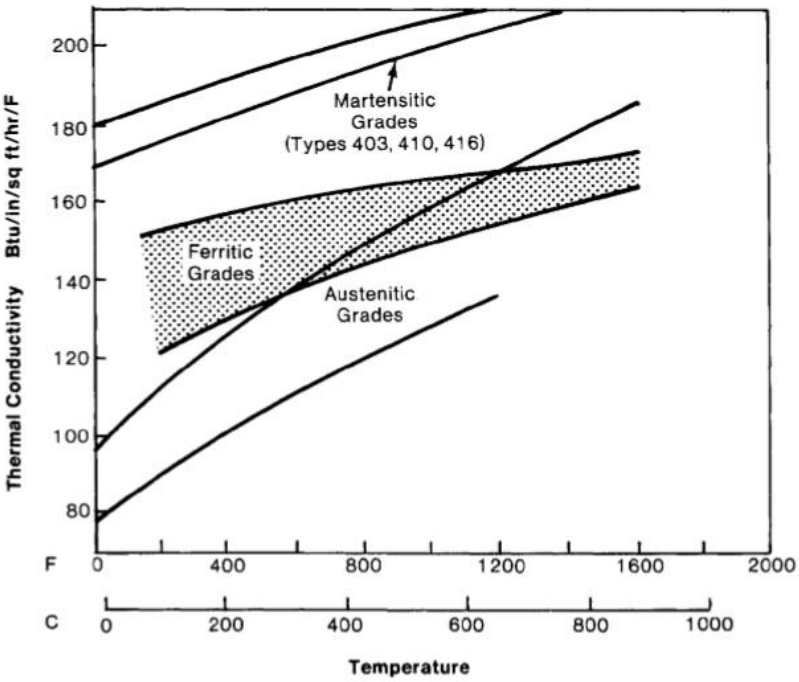

Figure 26
Tensile Modulus for Ferritic Steels (Alloy and Stainless) (10)

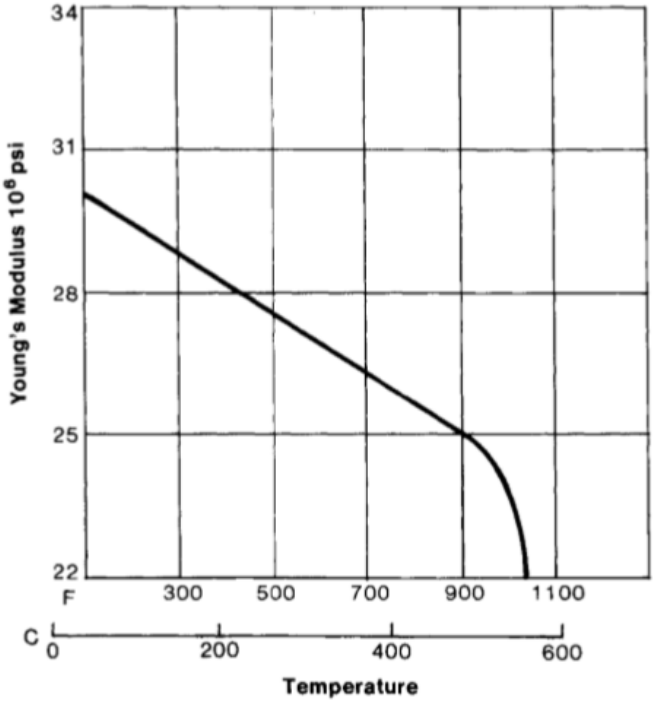

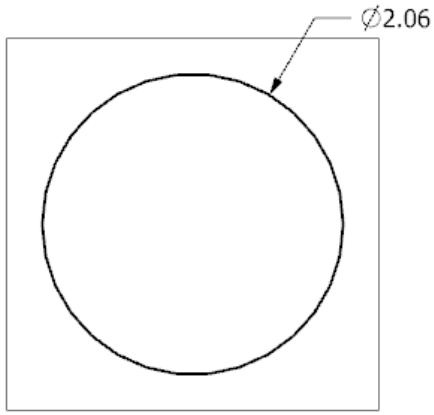

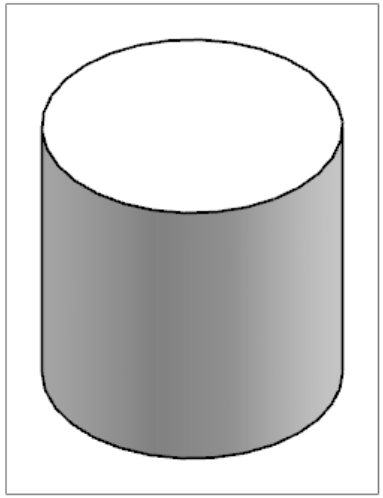

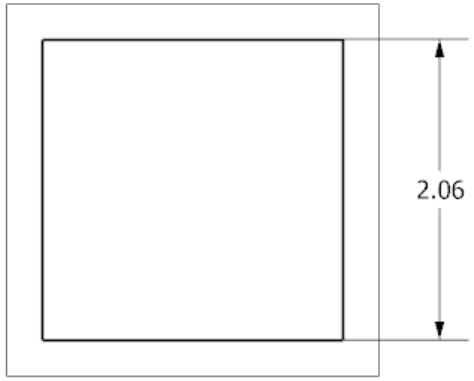

Quartz window

Scale 1:2

All dimensions are in 'inches'

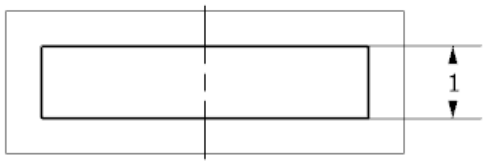

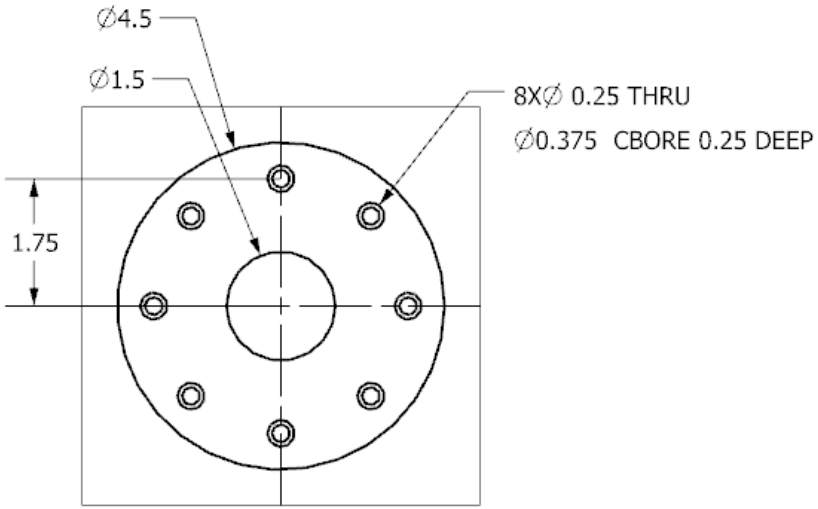

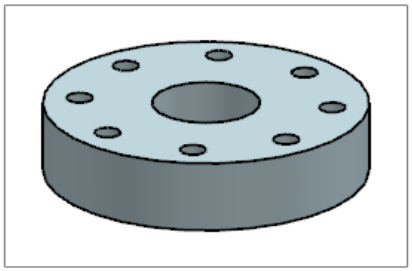

Circular Window Cover

Scale 1:2

All dimensions are in 'inches'

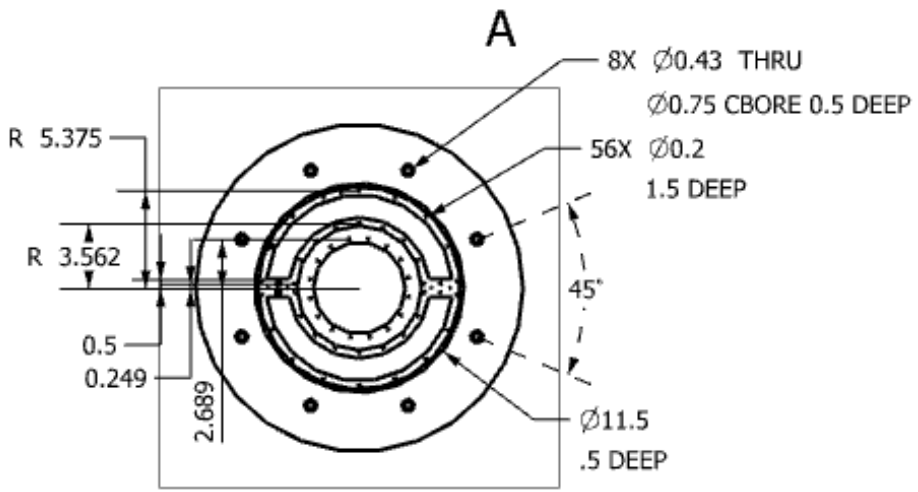

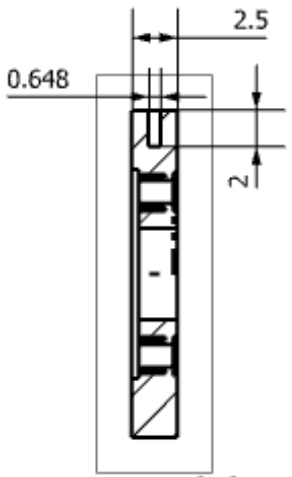

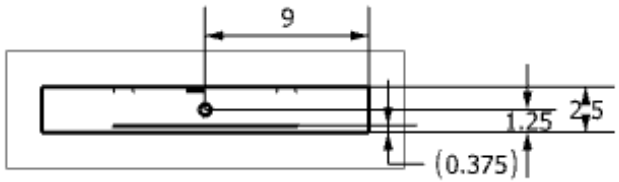

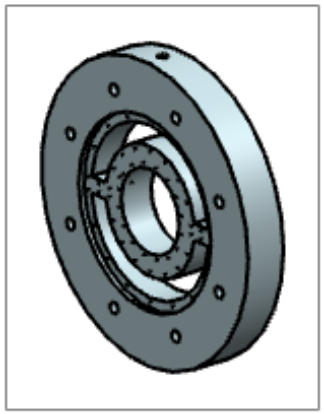

Front Cap, Updated 04/20/17

Scale 1:8

All dimensions are in 'inches'

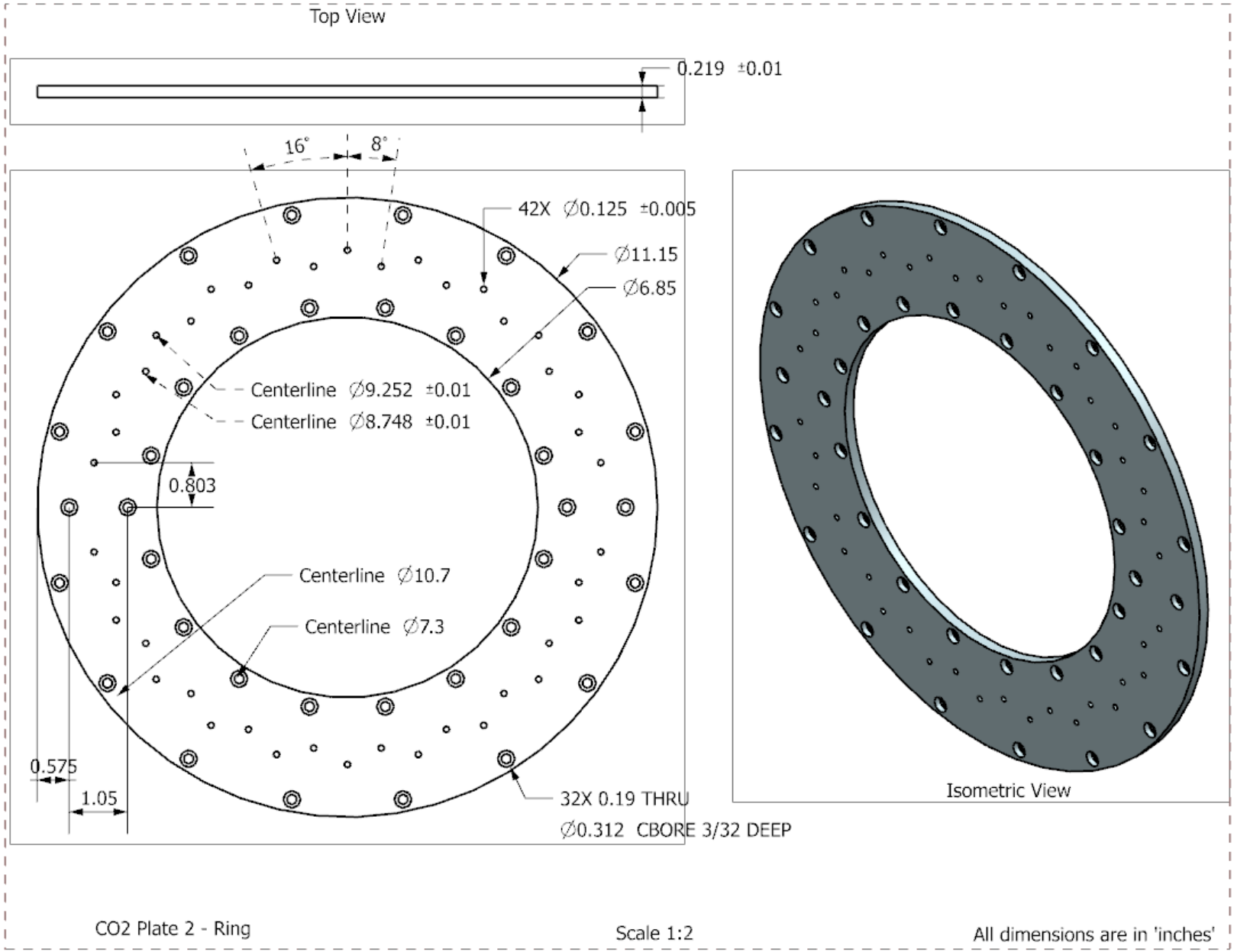
Top View
0.219 ±0.01
16°
8°
42X ∅0.125 ±0.005
∅11.15
∅6.85
Centerline ∅9.252 ±0.01
Centerline ∅8.748 ±0.01
0.803
Centerline ∅10.7
Centerline ∅7.3
0.575
1.05
32X 0.19 THRU
∅0.312 CBORE 3/32 DEEP
Isometric View
CO2 Plate 2 - Ring
Scale 1:2
All dimensions are in 'inches'

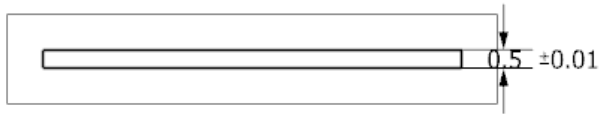

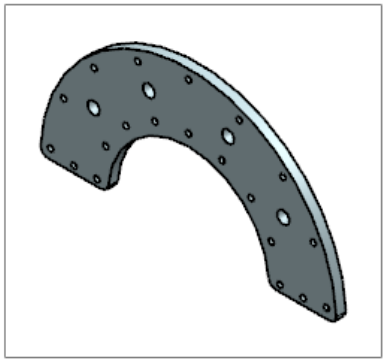

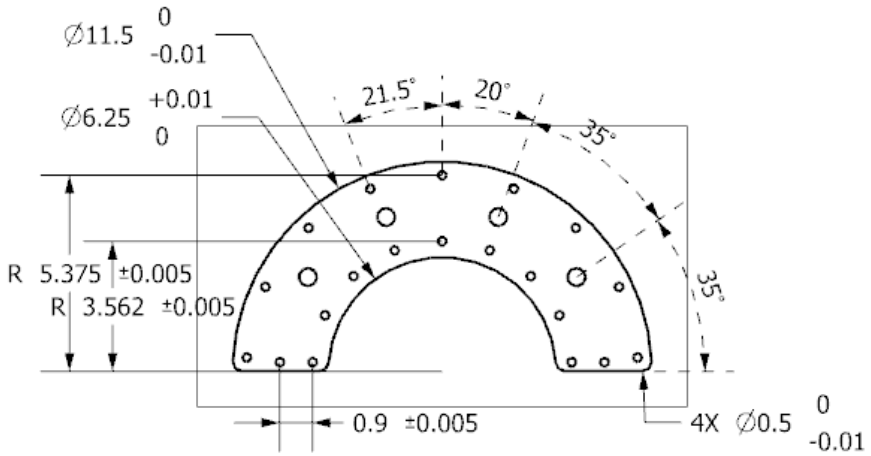

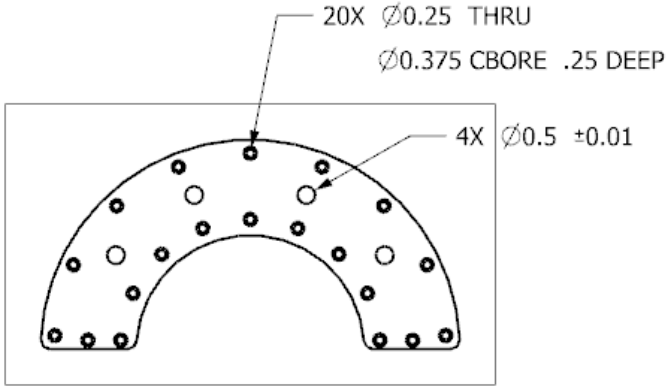

CO2 Plate 1

Scale 1:4

All dimensions are in 'inches'

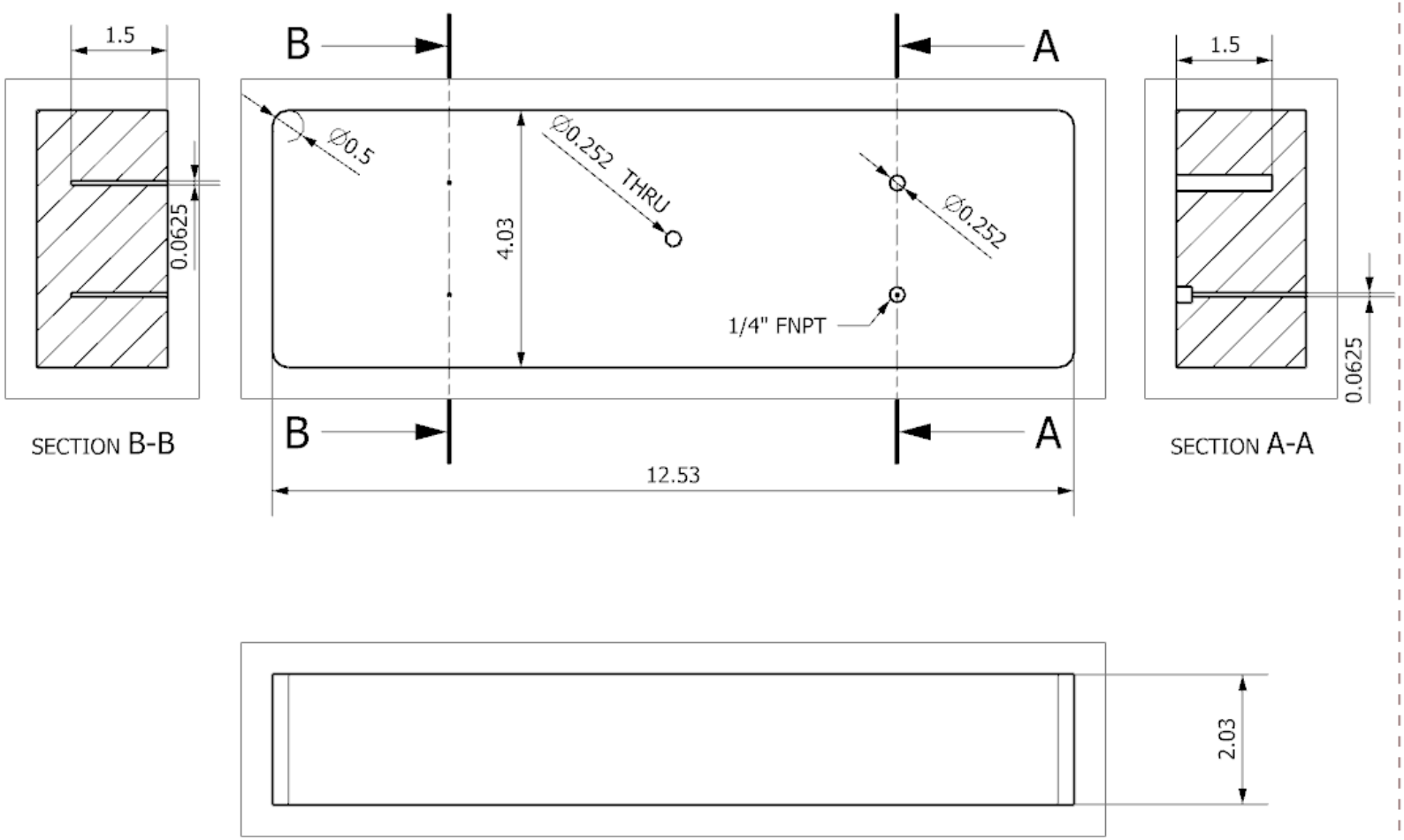

Metal Cover

Scale 1:2

All dimensions are in 'inches'

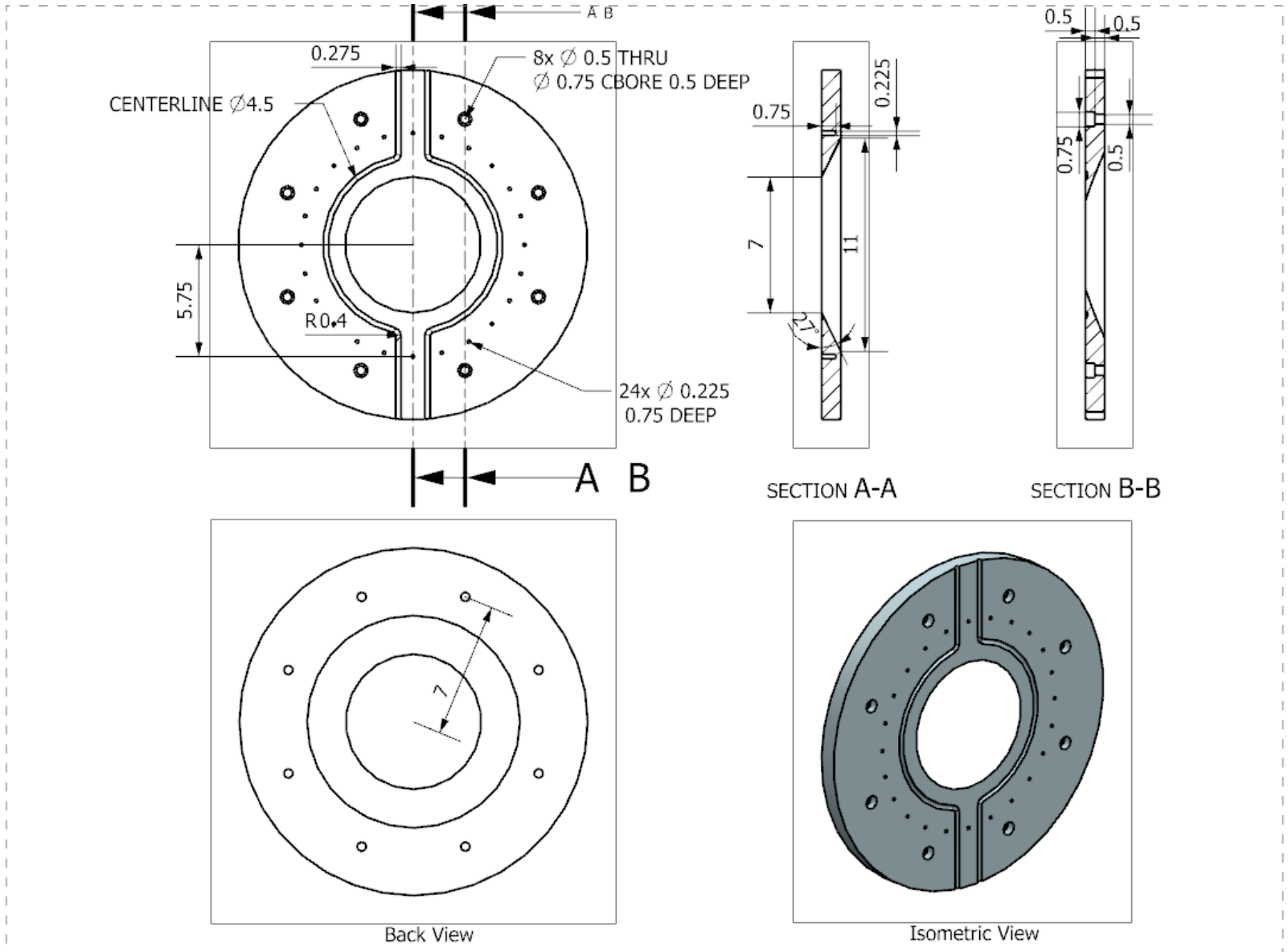
A B
0.275
8x ∅ 0.5 THRU
∅ 0.75 CBORE 0.5 DEEP
CENTERLINE ∅4.5
5.75
R0.4
24x ∅ 0.225
0.75 DEEP
A B
0.75
0.225
7
11
27°
SECTION A-A
0.5
0.5
0.75
0.5
SECTION B-B
7
Back View
Isometric View
End Cap-Part 1, Updated 04/20/17
Scale 1:6
All dimensions are in 'inches'

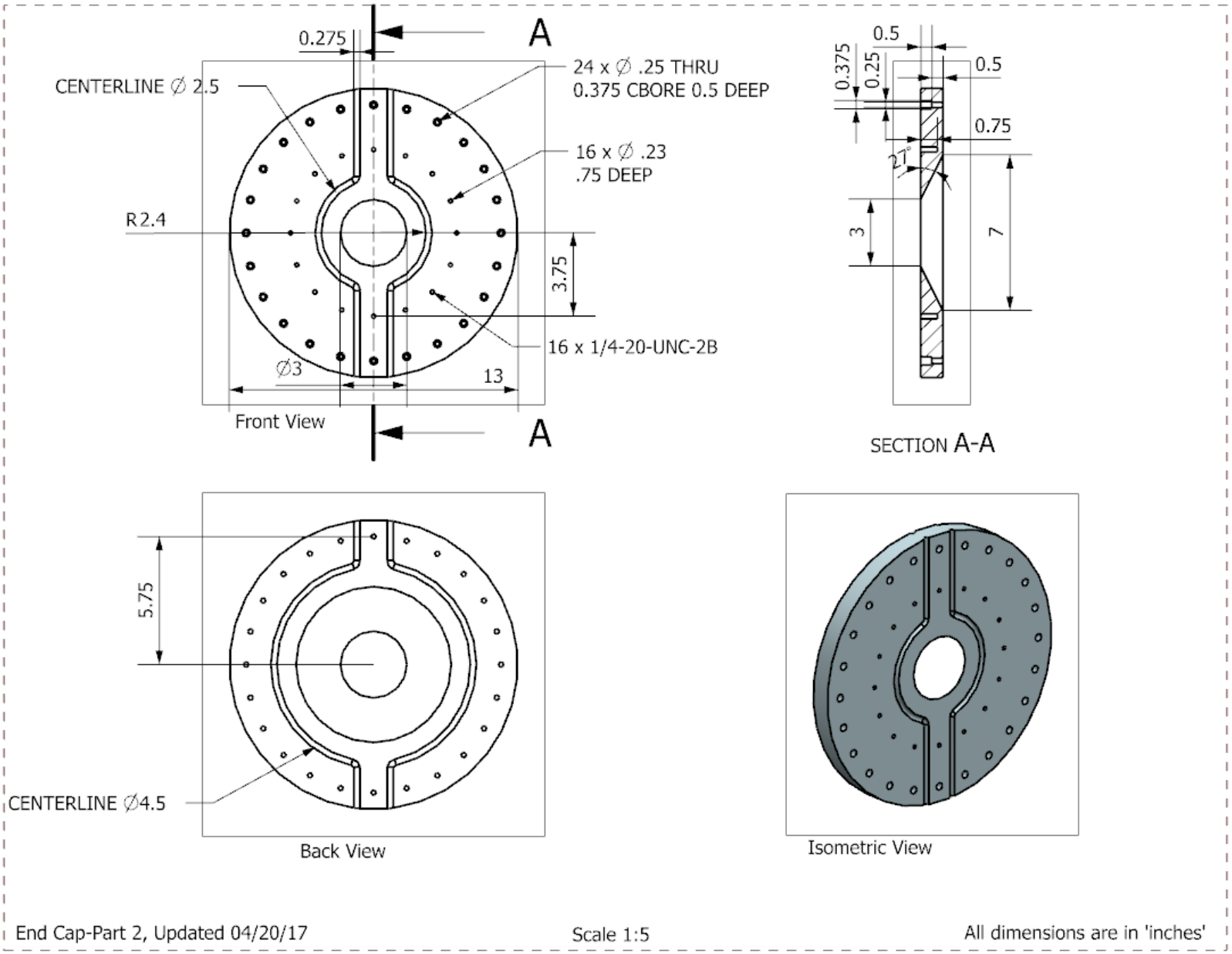
0.275
A
CENTERLINE ∅ 2.5
24 x ∅ .25 THRU
0.375 CBORE 0.5 DEEP
16 x ∅ .23
.75 DEEP
R2.4
3.75
16 x 1/4-20-UNC-2B
∅3
13
A
Front View
0.5
0.375
0.25
0.5
0.75
21°
3
7
SECTION A-A
5.75
CENTERLINE ∅4.5
Back View
Isometric View
End Cap-Part 2, Updated 04/20/17
Scale 1:5
All dimensions are in 'inches'

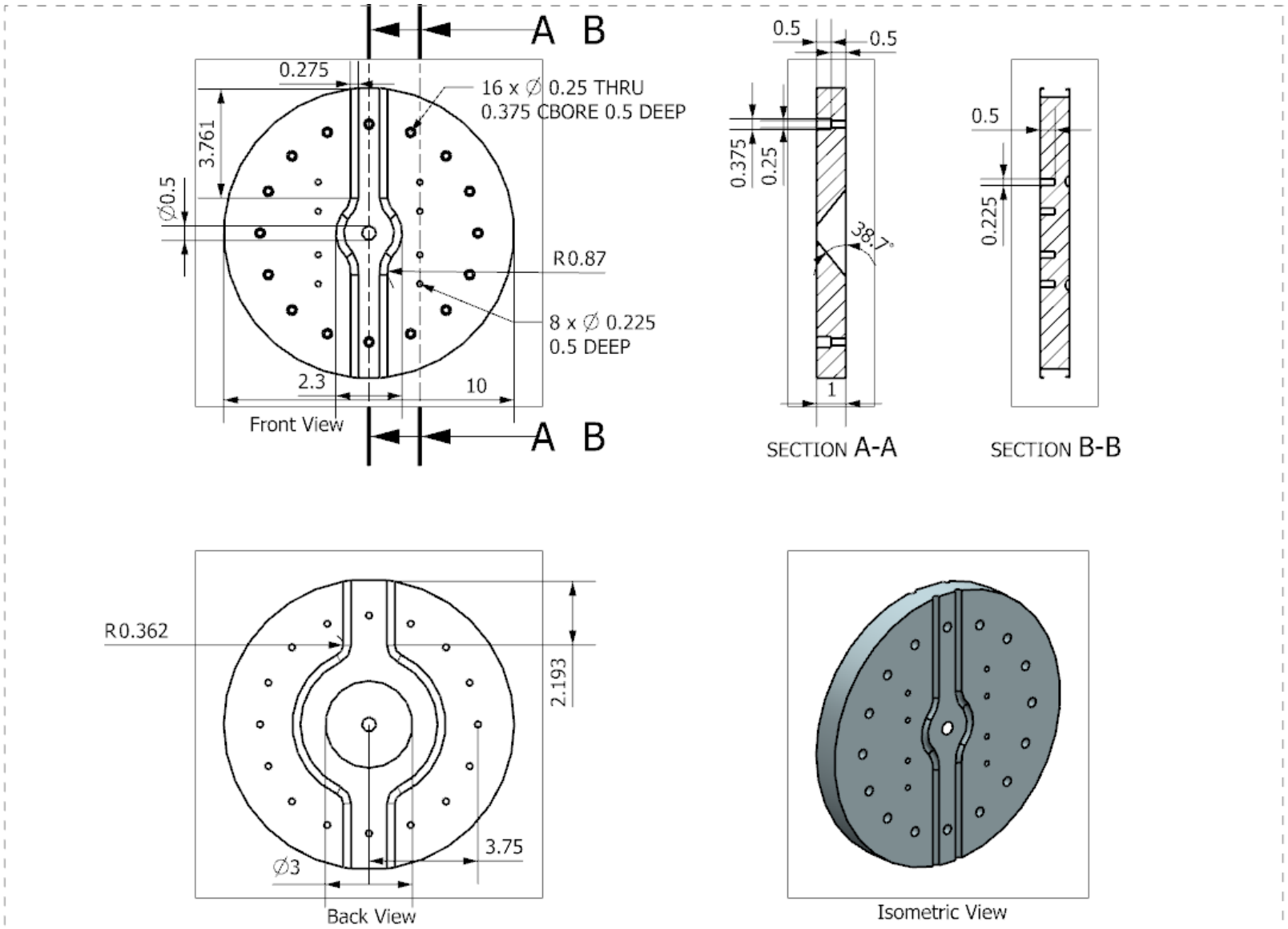

End Cap-Part 3, Updated 04/20/17 Scale 1:4 All dimensions are in 'inches'

Vita

Jaime Cruz Gurrola was born and raised in Torreon, Mexico. After finishing high school in 2010, he attended The University of Texas at El Paso (UTEP). He completed his undergraduate studies in Mechanical Engineering on December 2014 as Magna Cum Laude. Soon after graduating, he decided to join the graduate program in Mechanical Engineering at UTEP starting on January 2015. During his studies, he worked as the lab manager for the Lockheed Martin Lab and the 3D Printing Lab, both located at UTEP. He also worked as a lecturer for the Manufacturing Engineering Lab course for three semesters.

Jaime received a co-op with Intel Corporation working as an Experimental Mechanics Lab intern. His work during the internship resulted in a publication in the Journal of Electronic Packaging titled "High-temperature interfacial adhesion strength measurement in electronic packaging using the double cantilever beam method".

After completing the co-op, Jaime was offered a research assistant position at UTEP's Center for Space Exploration Technology Research (cSETR) under the supervision of Dr. Norman Love. His research focused on the design and development of a high-pressure oxy-fuel combustor. This technology aims to reduce greenhouse gas emissions from the burning of fossil fuels to generate electricity. After graduation, he seeks to find a job opportunity related to his field of study.

Contact Information: jcruz3@miners.utep.edu

This thesis was typed by Jaime Cruz Gurrola.